# Control of interface states at metal/6H-SiC(0001) interfaces

Tokuyuki Teraji* and Shiro Hara†
*National Institute of Advanced Industrial Science and Technology (AIST), 1-1-1 Umezono, Tsukuba, Ibraki 305-8568, Japan*
(Received 13 January 2003; revised manuscript received 24 July 2003; published 22 July 2004)

Metal/6H-SiC(0001) interfaces free of Fermi level pinning were formed by realizing well-ordered atomic arrangements and perfect termination of the surface atoms of SiC substrates. The surfaces and interfaces were investigated by electrical measurements, Auger electron spectroscopy, low energy electron diffraction, x-ray photoemission spectroscopy, scanning tunneling microscopy, and transmission electron microscopy. We used three different regimes for the surface treatments: (i) the conventional procedure of degreasing and HF dipping, (ii) thermal oxidation followed by HF dipping after (i), and (iii) immersion into boiling water after (ii). We found that the dependence of the Schottky barrier height on the metal work function changes drastically following these surface treatments. The Fermi level at the interface prepared using only treatment (i) was almost pinned at ~0.8 eV below the conduction band minimum. On the other hand, for the interfaces formed by treatments (ii) and (iii), the position of the interface Fermi level varied strongly with the metal work function. In particular, treatment (iii) approached the Schottky limit, with a density of interface states of $4.6 \times 10^{10}$ states$\cdot$cm$^{-2}\cdot$eV$^{-1}$. The surface characterization of the SiC surfaces formed by the Schottky-limit treatment (iii) indicated that the surface was atomically flat, the terraces of the surface was terminated by hydrogen atoms, and their step-edges were stable due to passivation by oxygen. An abrupt commensurate epitaxial connection at the Ti/SiC interface was found for treatment (iii), whereas the Ti/SiC interface obtained by employing treatment (i) had a disordered layer with a thickness of ~2 nm, which is the origin of the large density of interface states enough to pin the interface Fermi level.

DOI: 10.1103/PhysRevB.70.035312 PACS number(s): 73.30.+y, 73.20.−r, 81.65.−b

## I. INTRODUCTION

The Schottky barrier at metal/semiconductor interfaces, which is one of the most essential research subjects for electronic devices,[1,2] has been studied for around half a century. The controllability of the Schottky barrier height $\phi_b$ on a semiconductor, which is of scientific interest and technological importance, is expressed by a characteristic slope parameter $S_\phi(\equiv \partial\phi_b/\partial\phi_m)$,[3] where $\phi_m$ is the metal work function. Before the 1980's, experimental $S_\phi$ values[4–6] had been estimated mostly for covalent semiconductors, whose values ranged from 0.11 to 0.19 for Si and from 0.06 to 0.22 for GaAs. These are much less than unity that is referred to as the Schottky limit. In general, an $S_\phi$ value less than unity indicates the presence of a large number of interface states, since a high density of interface states reduces the width of the Fermi-level shift caused by the charge that cancels the work function difference between the semiconductor and the metal. Theoretically, there is a model that ascribes the main origin of the interface states to metal-induced gap states (MIGS). MIGS is interface states formed by modifying the semiconductor band due to the direct connection of the metallic wave function to the semiconducting wave function.[7–9] The degree of the modification, *that is*, the density and decay length of MIGS, was calculated to be inversely related to ionicity.[9] Actually, old tabulated barrier heights tell us that $S_\phi$ values for a highly-ionic semiconductor are larger than the values for the covalent semiconductors.[3,4] From this trend between the ionicity and $S_\phi$, the value of $S_\phi$ in a semiconductor material had been believed to be inherent to the semiconductor.[10]

In the 1980's advances in experimental techniques lead to findings of relations between $\phi_b$ and the interface structures in terms of atomic arrangements and chemical bonding. One of the most typical phenomena is a large change in barrier height by the change in geometrical connection between a metal and a semiconductor, which was found by Tung's experiment using the twin epitaxial $NiSi_2$/Si(111) system.[11] Another type of important experiment to illustrate the interface contribution to $\phi_b$ is to terminate the interface dangling bonds to reduce the density of the interface states, which is expected to raise the value of $S_\phi$. Lay *et al.*[12] obtained $\phi_b$ of 0.12 eV by depositing Pb on an $n$-Si(111) monohydride surface. This contrasts well with the conventional pinned barrier height of ~0.7 eV, implying a possibility of a wide change in $\phi_b$. Fan *et al.*[13] reported that $S_\phi$ increases from a conventionally reported value of 0.14 to a value of 0.53 by sulfur termination on an $n$-GaAs(100) surface. Brillson's group[14] deposited Au and Al onto $n$-GaAs(100) surfaces. They showed that a higher $S_\phi$ value is obtained by lowering the temperature during metal deposition. These results suggest that $S_\phi$ depends on the surface electronic states and/or the interface chemical reactivities as well as bulk properties, while MIGS is conceptually reasonable. In other words, both of MIGS and the states induced by the interface factors observed by the experiments are origins of the interface states and the resultant interface potential barrier. The degrees of their importance are the scientific issue.

In an ionic semiconductor, the MIGS effect to the interface dipole is lowered as mentioned already. This results in relatively larger effects of interface factors. In addition, since the ionic semiconductor has a strong binding energy originating from its higher ionicity, the interface tends to be thermally stable, and an interfacial chemical reaction that might be one of the origins of the interface states hardly progresses. As a result, the surface treatment for an ionic semiconductor

 ©2004 The American Physical Society

TABLE I. Cleaning procedures including a common pre-cleaning procedure (upper column) and additional procedures (lower column) referred to as the DHF, O/E, and BW procedures.

| | Common pre-cleaning procedure (degrease) | | |
|---|---|---|---|
| Dicing: | Samples ($3.75\times3.75$ mm$^2$) cut from a SiC wafer (some glue is used) ↓ | | |
| Glue removal: | Clean TCE dipping with stirring ~10 times until glue removal confirmed by optical microscope ↓ | | |
| Ultrasonic cleaning: | DI (5 min)→methanol (5 min)→TCE (10 min) →methanol (5 min)→DI (5 min) ↓ | | |
| SPM (optional): | (96% $H_2SO_4$:30% $H_2O_2$=4:1, 120 °C, 5 min→running water) | | |
| | DHF | O/E | BW |
| RCA cleaning (SC-1): | - | (29% $NH_4OH$:30% $H_2O_2$:$H_2O$ =1:1:5, 80±5 °C, 10 min) | (29% $NH_4OH$:30% $H_2O_2$:$H_2O$ =1:1:5, 80±5 °C, 10 min) |
| Diluted HF rinse: | 5% HF (10 min) | 5% HF (10 min)→DI (1 min) | 5% HF (10 min)→DI (1 min) |
| Thermal oxidation: | - | 1100 °C, 150 min, dry $O_2$ | 1100 °C, 150 min, dry $O_2$ |
| Diluted HF rinse: | - | 5% HF (10 min) | 5% HF (10 min)→DI (1 min) |
| Boiling water immersion: | - | - | DI (98 °C, 10 min) |
| DI rinse: | DI (1 min) | DI (1 min) | Running water |

becomes a dominant factor in generating the interface states and in determining the resultant $S_\phi$ compared to the situation in a covalent semiconductor. However, because of an insufficient amount of investigations on surfaces and interfaces, no systematical understanding of the effect of the surface and interfaces on $\phi_b$ and $S_\phi$ has been obtained.

At the end of the 1980's Baliga's group analyzed that optimum semiconductors for high-power electronics are wide gap semiconductors that tend to have high ionicities,[15] triggering extensive studies of the wide gap semiconductors with a view to using them in the practical field of electronic devices for power and high frequency. Since studies on SiC crystals and especially on SiC surfaces are the most advanced in the wide gap semiconductors,[16] the evaluation of $S_\phi$ for SiC crystals is very important as the first precise and practical knowledge on the metal/ionic-semiconductor interfaces, and especially investigations into the relationship between surface treatments and $\phi_b$.

$S_\phi$ values for 6H-SiC(0001) epitaxial films, which we estimate using the $\phi_b$ values reported by Waldrop *et al.*[17,18] and Porter *et al.*[19–22] are 0.670 and 0.140, respectively. In these experiments, the formation of thick oxidized layers followed by the removal of the oxidized layers has been carried out to remove any contaminated surface layers. However, low proportionalities were obtained between $\phi_b$ and $\phi_m$. These results imply that the development of an advanced surface treatment is required for an accurate estimation of $S_\phi$ in the metal/SiC interfaces. In this study, we introduce advanced surface treatments for the SiC surface in order to decrease the density of surface states. Then, we will show a wide variation of $S_\phi$ by utilizing these surface treatments. In addition, we demonstrate experimentally the formation of Schottky limit interfaces with drastically lower densities of interface states.

## II. EXPERIMENT

Commercially available nitrogen-doped *n*-type 6H-SiC(0001) epitaxial wafers, 1 in. in diameter and tilted 3.5° toward the $[11\bar{2}0]$ axis were used in this study. The wafer substrates were grown by the modified-Lely method and the epitaxial films with a thickness of 10 $\mu$m were deposited on them by chemical vapor deposition with feeding nitrogen as *n*-type doping gas. The carrier concentration estimated from the capacitance-voltage ($C-V$) method was $5\times10^{17}$ cm$^{-3}$. All sample cleaning procedures are summarized in Table I. Samples cut to a size of $3.75\times3.75$ mm$^2$ were degreased and then dipped in 5% HF solution. This cleaning process is referred to as DHF treatment. Some samples after the degrease were cleaned using the SC-1 procedure of RCA cleaning.[23] After dipping into 5% HF solution followed by rinsing in deionized water (DI), the samples were thermally oxidized in a quartz tube furnace at 1100 °C for 150 min using dry oxygen gas. No pile-up of nitrogen atoms at the oxide/SiC interface was observed by secondary ion mass spectroscopy. The oxidized layer, 10 nm in thickness, was then etched by 5% HF solution. We will refer to this sequence of treatment as O/E treatment hereafter. It is reported that an as-received 6H-SiC(001) substrate with a surface layer exhibiting no low-energy electron diffraction (LEED) spot can be improved to have a sharp $(1\times1)$ pattern by thermal oxidation followed by dipping in hydrofluoric acid.[24] After O/E treatment, some of the samples were immersed in boiling water at 98 °C for 10 min. This sequence of treatment will be referred to as BW treatment. It is known that the Si(111) surface is terminated by monohydride when it is dipped into boiling water that has a reduced concentration of dissolved oxygen.[25,26] In our experiment, deionized water without any intentional control of oxygen concentration was used. A typical value of dissolved oxygen in DI was

in ~3 to 4 ppm. The resistivity of the water was 18.2 $M\Omega \cdot cm$, and a typical concentration of total organic carbon was around 10 ppb. All samples were rinsed in the deionized water.

A metal was deposited onto the SiC epitaxial surface after each surface treatment, using an *e*-beam evaporator with a base pressure of $\sim 4\times10^{-11}$ Torr. Deposited metals were Ti, Mo, Ni, Pt, and Al. Electrodes 150 $\mu$m in diameter and 500 nm in typical thickness were formed on the samples through Mo masks. Each sample had over 20 electrodes. During the depositions there was no intentional sample heating. The maximum sample temperature during the Mo deposition was 150 °C, and sample temperatures during the other metal depositions were below 100 °C. After the Schottky electrode formation, Mg was evaporated as the back Ohmic electrodes, without any additional thermal treatment. The average specific contact resistivity of the Mg-Ohmic electrodes was around $10^{-2}$ $\Omega \cdot cm^2$, which is sufficiently low for evaluating the Schottky barrier heights in current-voltage ($I-V$) and $C-V$ measurements. Note that an Ohmic contact formation prior to a Schottky contact formation contaminates the surface for the Schottky contact, leading to a deterioration of the Schottky interface. Conventionally, an Ohmic contact on SiC crystals is formed by Ni deposition and subsequent annealing at >1000 °C. This high-temperature process affects the quality of the surface for the Schottky contact. In order to form a controllable Schottky barrier height, the Ohmic contact must be formed without contaminating the Schottky surface, and without any thermal effect to the Schottky electrode.

### III. ELECTRIC PROPERTIES

Schottky barrier heights at the metal/SiC interfaces were estimated from both $I-V$ and $C-V$ measurements. The measurement systems were a picoammeter (HP 4140B) and a capacitance meter (HORIBA DA-1500). Electrical measurements were carried out at room temperature in a box shielded from the light.

The electrical characteristic at the metal/semiconductor interface is expressed by the potential distribution with a barrier peak and the current transport over and through the barrier. In a homogeneous dopant distribution, the potential distribution has the form of the second order for a distance. The current density $J$ for an *n*-type semiconductor over this potential barrier is expressed in the following equation called the thermionic emission theory[2] originally described by Bethe:[27]

$$J=J_S\left[\exp\left(\frac{qV}{kT}\right)-1\right], \tag{1}$$

where

$$J_S=A^*T^2\exp\left(-\frac{q\phi_{bn}}{kT}\right). \tag{2}$$

Here, $A^*$ is the Richardson constant, $T$ the absolute temperature, $\phi_{bn}$ a measured raw Schottky barrier height with a bias voltage $V$, $k$ the Boltzmann constant, and $q$ the elementary charge. $A^*$ of the 6H-SiC(0001) crystal used is 194.4 $A\cdot cm^{-2}\cdot K^{-2}$.[20] In a practical interface, a modified equation $(1')$ with the ideality factor $n$ is used to describe the measured $I-V$ characteristic under a simple assumption that there is a kind of bias-dependent leakage current as well as the constant reverse current $J_s$:[2]

$$J=J_S\left[\exp\left(\frac{qV}{nkT}\right)-1\right]. \tag{1'}$$

The measured barrier height $\phi_{bn}$ is a barrier height lowered by the image force at the interface, compared with the barrier height $\phi_{b0}$ whose barrier has the simple second-order potential curve.[27] This is expressed by the following equation:

$$\phi_{b0}^{IV}=\phi_{bn}+\Delta\phi. \tag{3}$$

Here, $\Delta\phi$ is the image force lowering and the notation *IV* indicates that the barrier height is obtained from $I-V$ measurement. $\Delta\phi$ is expressed by the following equation:[1]

$$\Delta\phi=\left[\frac{q^3N_D(V_b-kT/q)}{8\pi^2\varepsilon_s(\varepsilon_s')^2}\right]^{1/4}, \tag{4}$$

where $V_b$ is the built-in potential, $N_D$ is the donor density, $\varepsilon_s$ is the static permittivity of a semiconductor and $\varepsilon_s'$ is the dynamic permittivity. In this study, we use the values of $10.03\varepsilon_0$ for $\varepsilon_s$,[28] and $6.8\varepsilon_0$ for $\varepsilon_s'$.[29] $V_b$ is calculated from $V_b=\phi_{bn}-V-V_n$ where $V_n$ is the energy difference between the bottom of the conduction band and the Fermi-level of the semiconductor. $V_n$ is calculated using a graphical method described in Ref. 2. Using $2.1\times10^{19}$ $cm^{-3}$ for $N_C$ the effective density of states in the conduction band at 300 K,[30] $-0.081$ eV for $E_D$ the nitrogen donor level of the *h* site in the 6H-SiC crystal,[31] and $5\times10^{17}$ $cm^{-3}$ for $N_D$, then $V_n$ becomes 0.11 V.

In the $C-V$ measurements, the Schottky barrier height $\phi_b^{CV}$ is given by

$$\phi_b^{CV}=V_{bi}+V_n-\frac{kT}{q}, \tag{5}$$

where $V_{bi}$ is the voltage intercept on the voltage axis in the graph of $1/C^2$ vs $V$. At the intercept, the band has a zero space charge region and the band is flat.[2] The barrier height $\phi_b^{CV}$ obtained from the intercept without calculating $\Delta\phi$ is called the flat-band barrier height. One can compare $\phi_b^{CV}$ and $\phi_{b0}^{IV}$ as similar barrier-height parameters that have no lowering by the image force.

Using the above equations, measured data, $\phi_{bn}$, $n$, and $V_{bi}$ in this paper were converted to $\phi_{b0}^{IV}$, $n$, and $\phi_b^{CV}$. These converted data collected from many electrodes were averaged every cleaning treatment and metal. The mean values $\langle\phi_{b0}^{IV}\rangle$ of the Schottky barrier heights and the mean values $\langle n\rangle$ of the ideality factors obtained by the $I-V$ measurements of the electrodes are summarized in Table II. The Schottky barrier heights in the parentheses in the table are mean values $\langle\phi_{b0}^{IV}\rangle$ averaged from $\phi_{b0}^{IV}$ for all the measured electrodes. Errors in the barrier heights in our experiments are defined as the standard deviation $1\sigma$.

TABLE II. Mean values of Schottky barrier heights $\langle \phi_{b0}^{IV} \rangle$ and ideality factors $\langle n \rangle$ of metal/6H-SiC(0001) electrodes for five metals and for the three cleaning procedures. $\sigma$ is the standard deviation of each mean value. $\langle \phi_{b}^{CV} \rangle$ for BW samples are displayed on the right side in the table.

| Metal | $I$-$V$ DHF $\langle \phi_{b0}^{IV} \rangle \pm \sigma$ (V) ($\langle n \rangle \pm \sigma$) | $I-V$ O/E $\langle \phi_{b0}^{IV} \rangle \pm \sigma$ (V) ($\langle n \rangle \pm \sigma$) | $I$-$V$ BW $\langle \phi_{b0}^{IV} \rangle \pm \sigma$ (V) ($\langle n \rangle \pm \sigma$) | $C-V$ BW $\langle \phi_{b}^{CV} \rangle \pm \sigma$ (V) |
|---|---|---|---|---|
| Al | $0.728 \pm 0.003$ | $0.443^{+0.014}_{-0.036}$ | $0.435^{+0.003}_{-0.005}$ | |
| | $(2.70 \pm 0.12)$ | | | |
| Ti | $0.736 \pm 0.04$ | $0.561 \pm 0.032$ | $0.451 \pm 0.003$ | |
| | $(1.25 \pm 0.18)$ | $(1.21 \pm 0.12)$ | | |
| Mo | $0.708 \pm 0.004$ | $0.780 \pm 0.029$ | $0.808 \pm 0.007$ | $0.840 \pm 0.005$ |
| | $(1.10 \pm 0.01)$ | $(1.21 \pm 0.10)$ | $(1.11 \pm 0.02)$ | |
| Ni | $0.891 \pm 0.004$ | $1.030 \pm 0.013$ | $1.186 \pm 0.038$ | $1.259 \pm 0.015$ |
| | $(1.09 \pm 0.01)$ | $(1.50 \pm 0.04)$ | $(1.25 \pm 0.07)$ | |
| Pt | $0.926 \pm 0.006$ | $1.149 \pm 0.030$ | $1.324 \pm 0.087$ | $1.772 \pm 0.017$ |
| | $(1.32 \pm 0.02)$ | $(1.55 \pm 0.05)$ | $(1.60 \pm 0.17)$ | |

The $\langle \phi_{b0}^{IV} \rangle$ data in Table II are plotted in Fig. 1 as a function of the metal work function $\phi_m$.[32] $\langle \phi_{b0}^{IV} \rangle$ increases with increasing $\phi_m$ in each surface treatment. The fitting lines in Fig. 1 were calculated by the least squares method. $S_\phi$ for DHF, O/E, and BW samples, which are the slopes of each line, are 0.180, 0.549, and 0.754, respectively. These $S_\phi$ values are much less than unity. In Table II, $\langle n \rangle$ values are much larger than $n=1$ for the ideal thermionic emission theory in Eqs. (1) and (2). $n>1$ is often called a leakage current apparently. However, it originates from various kinds of complex current transport phenomena, such as the tunneling current, the recombination current, the edge-leakage current, and so on,[2] which has been analyzed as an inhomogeneous distribution of barrier heights.[33–37] Also, it was reported that $n$ has a strong relation to Schottky barrier heights measured by $I-V$.[33–35] In a report on Ir/Si interfaces,[33] the Schottky barrier height was initially plotted versus $n$, as far as we are aware. Later, a close relationship between $\phi_b - n$ was demonstrated for Ag electrodes on the $7 \times 7$ reconstruction on the Si(111) substrate.[34] Recently, the $\phi_b - n$ plot was used to explain the inhomogeneous distribution of barrier heights of Ti/4H-SiC rectifiers.[35] According to these reported data, the barrier height inhomogeneity tends to lower the barrier height observed by the $I-V$ measurement. This suggests a possible underestimation of $S_\phi$ when $n>1$.

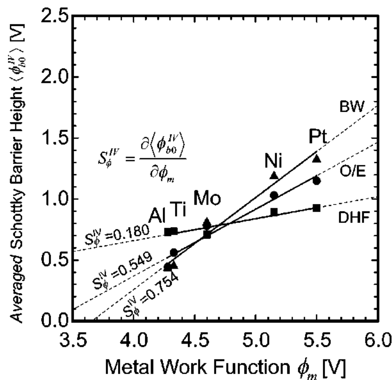


FIG. 1. Averaged values of Schottky barrier heights $\langle \phi_{b0}^{IV} \rangle$ obtained from $I-V$ measurements at metal/6H-SiC(0001) electrodes as a function of the metal work function $\phi_m$. $S_\phi$ for DHF, O/E, and BW samples obtained from slopes $\partial \langle \phi_{b0}^{IV} \rangle / \partial \phi_m$ are 0.180, 0.549, and 0.754, respectively. Detailed cleaning procedures of the DHF, O/E, and BW samples are listed in Table I.

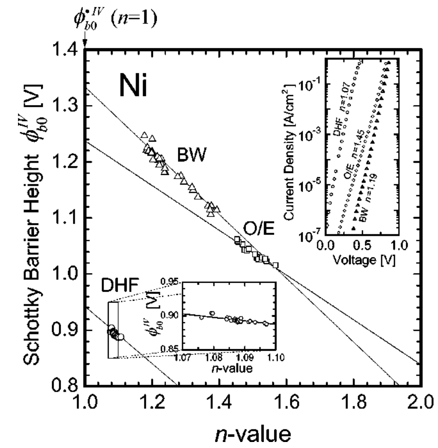


FIG. 2. Schottky barrier heights $\phi_{b0}^{IV}$ of Ni/6H-SiC(0001) electrodes as functions of the ideality factor $n$. Note that these electrodes in each treatment are formed at the same time on each treated sample surface. Even in each identical sample cleaning conditions, the value of $n$ or the leakage current have large variations, but the electrodes have unique ideal values at $n=1$. The ideal barrier height $\phi_{b0}^{\cdot IV}$, which is obtained by extrapolating the plots using the least squares method for DHF, O/E, and BW samples are 0.939 V, 1.238 V, and 1.331 V, respectively. The insets show $I-V$ characteristics with a minimum $n$ in each treatment and magnified $\phi_{b0}^{IV} - n$ plots of the DHF-treated sample.

Figure 2 shows $\phi_{b0}^{IV}$ at Ni/6H-SiC(0001) interfaces as functions of the surface treatments. The insets of Fig. 2 are $I-V$ characteristics with a minimum $n$ in each treatment, and magnified $\phi_{b0}^{IV} - n$ plots of a DHF-treated sample. The smallest $n$ value of the DHF electrodes is 1.076. The plots of the DHF electrodes are concentrated at around 0.89 V, and have an $\langle n \rangle$ of 1.09. This concentration of the plots will be discussed in Sec. VI. The $n$ values of the O/E and BW electrodes are spreading, suggesting no dominant local interface states at any level. $\langle n \rangle$ for the BW electrodes is smaller than that of the O/E electrodes. In all treatments, there are strong linear relationships between $\phi_{b0}^{IV}$ and $n$. Note that these electrodes were formed at the same time on each treated sample surface. Even for identical sample cleaning conditions for the over 20 electrodes on each sample, $n$ has large variations. But owing to the linear relations with $\phi_{b0}^{IV}$ ideal barrier heights are obtained by extrapolating lines calculated from the least square method to $n=1$. We define the ideal barrier height $\phi_{b0}^{IV}$ at $n=1$ as $\phi_{b0}^{\cdot IV}$. The lines calculated from the method are depicted by straight lines for each treatment in Fig. 2. $\phi_{b0}^{\cdot IV}$ for the DHF, O/E, and BW samples are $0.939 \pm 0.006$ V, $1.238 \pm 0.013$ V, and $1.331 \pm 0.006$ V, respectively.

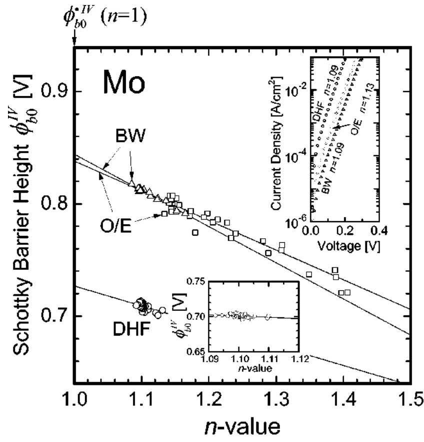

FIG. 3. $\phi_{b0}^{IV}$ of Mo/6H-SiC(0001) electrodes as functions of $n$. $\phi_{b0}^{\cdot IV}$ for DHF, O/E, and BW samples are 0.727 V, 0.838 V, and 0.844 V, respectively. The insets show $I-V$ characteristics with a minimum $n$ in each treatment and magnified $\phi_{b0}^{IV}-n$ plots of the DHF-treated sample.

$\phi_{b0}^{IV}-n$ plots of Mo/SiC interfaces are shown in Fig. 3. The insets in Fig. 3 show $I-V$ characteristics with a minimum $n$ in each treatment and magnified $\phi_{b0}^{IV}-n$ plots of DHF-treated electrodes. $n$ of the DHF electrodes concentrates around $1.10\pm0.01$, while those of the O/E and BW electrodes spread. $\langle n\rangle$ of the O/E electrodes is larger than that of the BW electrodes. These features are the same as those in the Ni electrodes. $\phi_{b0}^{\cdot IV}$ at Mo/SiC interfaces for the DHF, O/E, and BW electrodes are $0.727\pm0.003$ V, $0.838\pm0.002$ V, and $0.844\pm0.002$ V, respectively.

Figure 4(a) shows $\phi_{b0}^{IV}-n$ plots of Ti/SiC interfaces for DHF and O/E treatments. The inset in the figure shows $I-V$ characteristics at these interfaces with minima of $n$. $\phi_{b0}^{\cdot IV}$ for the O/E electrodes is much lower than that of the DHF electrodes. $\phi_{b0}^{\cdot IV}$ of the DHF and O/E electrodes are $0.786\pm0.005$ V and $0.581\pm0.008$ V, respectively. The barrier height $\langle\phi_{b0}^{IV}\rangle$ of the DHF electrodes is relatively comparable to the reported values of 0.73 V in Ref. 18. For BW electrodes, the $I-V$ characteristics show Ohmic properties, as shown in the inset in Fig. 4(b). The specific contact resistivity $\rho_c$ was estimated to be $(5.97\pm0.61)\times10^{-3}$ $\Omega\cdot\text{cm}^2$ from the extrapolated resistance $2R_c$ at zero distance in the figure. In the order of $10^{-3}$ $\Omega\cdot\text{cm}^2$, this kind of the simple electrode structure is enough to estimate $\rho_c$. In the thermionic emission transport, $\rho_c$ is expressed by[2]

$$\rho_C=\frac{k}{qA^*T}\exp\left(\frac{q\phi_{bn}}{kT}\right). \quad (6)$$

From Eqs. (3) and (6), $\phi_{b0}^{IV}$ for the Ti/SiC interface of the BW electrodes is $0.451\pm0.003$ V. Note that in our previous reports[38,39] we showed only $\phi_{bn}^{IV}$, not $\phi_{b0}^{IV}$ for Ti/SiC barrier heights. We have also improved the base pressure of our $e$-beam evaporator by three orders compared with the previous studies and suppressed outgassing during evaporation to achieve $\leqslant 1\times10^{-9}$ Torr. $\phi_{b0}^{IV}$ of Al electrodes with Ohmic properties in O/E and BW treatments were estimated to be

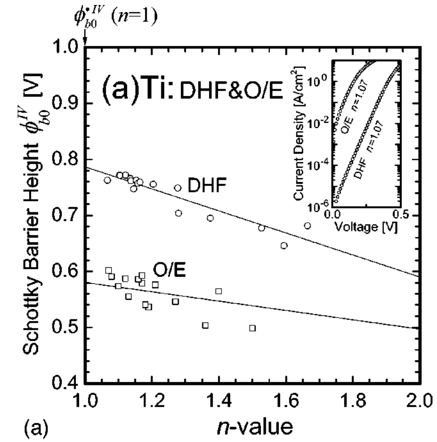

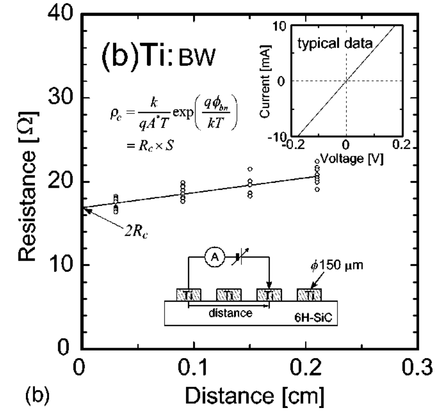

FIG. 4. (a) $\phi_{b0}^{IV}$ of Ti/6H-SiC(0001) electrodes as functions of $n$. $\phi_{b0}^{\cdot IV}$ for DHF and O/E samples are 0.786 V and 0.581 V, respectively. The inset shows $I-V$ characteristics with a minimum $n$ in each treatment. (b) Resistances between two Ti electrodes for BW samples as a function of the electrode distance. The specific contact resistivity $\rho_c$ obtained from the extrapolated resistance $2R_c$ is $(5.97\pm0.61)\times10^{-3}$ $\Omega\cdot\text{cm}^2$. The inset shows a typical $I-V$ characteristic for the Ti Ohmic electrodes.

$0.443^{+0.014}_{-0.036}$ V and $0.435^{+0.003}_{-0.005}$ V by the same procedure as that of the Ti Ohmic electrodes. As found in Figs. 2 to 4, the slopes of the $\phi_{b0}^{IV}-n$ relationships tend to decrease with decreasing $\langle\phi_{b0}^{IV}\rangle$. In other words, the dependence of $\phi_{b0}^{IV}$ on $n$ becomes weaker for interfaces with a lower barrier height. Since $\phi_{b0}^{\cdot IV}$ is not available for the low barrier heights obtained from Eq. (6), we approximate $\phi_{b0}^{IV}$ as $\phi_{b0}^{\cdot IV}$.

Using the whole data set of $\phi_{b0}^{\cdot IV}$ shown in Table III instead of $\langle\phi_{b0}^{IV}\rangle$ in Table II, we plot the relationship between the Schottky barrier heights and the metal work function $\phi_m$ in Fig. 5. Strong linearity is observed between $\phi_{b0}^{\cdot IV}$ and $\phi_m$ as shown in all the three lines. The correlation coefficients $r$ for DHF, O/E, and BW plots are 0.928, 0.983, and 0.996, respectively. It should be noted that all the plots including the barrier heights estimated from the Ohmic resistances in the Ti and Al electrodes have such strong linearity. This suggests that the thermionic emission mechanism and not the tunneling mechanism is applicable to the Ohmic interfaces. The slope parameters $S_{\phi}^{\cdot IV}$ obtained from $S_{\phi}^{\cdot IV}=\partial\phi_{b0}^{\cdot IV}/\partial\phi_m$ are shown in Table IV. $S_{\phi}^{\cdot IV}$ of the DHF, O/E, and BW electrodes are 0.215, 0.739, and 0.994, respectively. These values

TABLE III. The ideal barrier height $\phi_{b0}^{\cdot IV}$ of the metal/6H-SiC(0001) electrodes. Here superscript $\cdot$ indicates $\phi_{b0}^{IV}$ at $n=1$.

| Metal | $I-V$ DHF $\phi_{b0}^{\cdot IV}\pm\sigma$ (V) | $I-V$ O/E $\phi_{b0}^{\cdot IV}\pm\sigma$ (V) | $I$-$V$ BW $\phi_{b0}^{\cdot IV}\pm\sigma$ (V) |
|---|---|---|---|
| Al | $0.759\pm0.004$ | | |
| Ti | $0.786\pm0.005$ | $0.581\pm0.008$ | |
| Mo | $0.727\pm0.003$ | $0.838\pm0.002$ | $0.844\pm0.002$ |
| Ni | $0.939\pm0.006$ | $1.238\pm0.013$ | $1.331\pm0.006$ |
| Pt | $1.011\pm0.015$ | $1.365\pm0.024$ | $1.632\pm0.007$ |

are larger than $S_{\phi}^{IV}$ obtained from $S_{\phi}^{IV}=\partial\langle\phi_{b0}^{IV}\rangle/\partial\phi_m$. $\sigma$ in Table IV is the standard deviation of $S_{\phi}^{\cdot IV}$. For the BW interface, $\sigma$ divided by $S_{\phi}^{\cdot IV}(=\sigma/S_{\phi}^{\cdot IV})$ is the smallest in the three treatments, indicating a stronger relation between $\phi_{b0}^{\cdot IV}$ and $\phi_m$ than those in the DHF and O/E electrodes.

The inset in Fig. 5 shows the distribution of the density of interface states $D_{it}$ as a function of the energy from the conduction minimum $E_c$. Since the measured range of $\phi_{b0}^{\cdot IV}$ of the DHF electrodes is 0.26 eV in width from 0.74 eV to 1.00 eV, $D_{it}$ is evaluated only over this limited energy range as a direct estimation. For the O/E electrodes there is strong linearity in the $\phi_{b0}^{\cdot IV}-\phi_m$ relationship over a wider measured range of 0.90 eV, indicating that $D_{it}$ is constant over this range. In such a system with a constant $D_{it}$ that is independent of the metal, one can estimate $D_{it}$ for each surface treatment using the following equation proposed by Cowley and Sze:[40]

$$S_{\phi}^{\cdot}=\frac{\varepsilon_i}{\varepsilon_i+q^2\delta D_{it}}, \quad (7)$$

where $\varepsilon_i$ is the permittivity of the interfacial layer and $\delta$ is the width of the interface layer. As in the original paper of Ref. 40, a permittivity value of $8.854\times10^{-14}$ F$\cdot$cm$^{-1}$ in a vacuum was used as $\varepsilon_i$. $\delta$ was assumed to be one bilayer-spacing of 0.25 nm on the 6H-SiC(0001) substrate.[41] Using $S_{\phi}^{\cdot}$ in Eq. (7), $D_{it}$ for the DHF, O/E, and BW electrodes are $2.80\times10^{13}$, $2.71\times10^{12}$, and $4.63\times10^{10}$ states$\cdot$cm$^{-2}\cdot$eV$^{-1}$, respectively. Even if we use the lower limit $S_{\phi}^{\cdot}-\sigma$ of 0.941 $(=0.994-\sigma)$ for BW, the calculated value is $4.81\times10^{11}$ states$\cdot$cm$^{-2}\cdot$eV$^{-1}$. The upper limit, 1.047 $(=0.994+\sigma)$ is out of range in Eq. (7), corresponding to a zero density of interface states. The very low density of interface states obtained, $4.63\times10^{10}$ states$\cdot$cm$^{-2}\cdot$eV$^{-1}$, indicates that all kinds of possible states, including MIGS, are definitely ineffective in terms of the interface $E_F$ pinning, at least in our experimental range, which is 1.2 eV in width from Al to Pt. Practically, in terms of the barrier height control, the BW interface is in the Schottky limit condition.

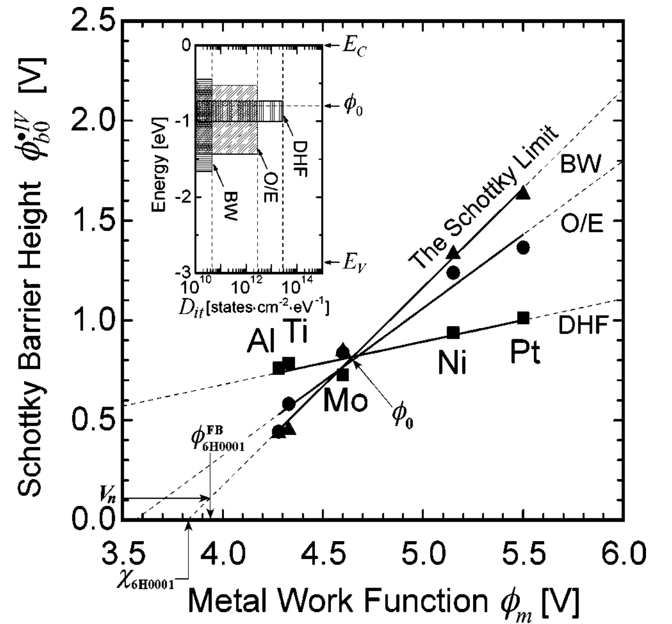


FIG. 5. The relationship between the ideal barrier height $\phi_{b0}^{\cdot IV}$ (where the superscript $\cdot$ indicates $\phi_{b0}^{IV}$ at $n=1$), and the metal work function $\phi_m$ for the three different surface treatments DHF, O/E, and BW. Strong linearity is observed between $\phi_{b0}^{\cdot IV}$ and $\phi_m$ in the three lines. $S_{\phi}^{\cdot IV}(=\partial\phi_{b0}^{\cdot IV}/\partial\phi_m)$ for DHF, O/E, and BW treatments are 0.215, 0.739, and 0.994, respectively. The inset shows the distribution of $D_{it}$ calculated using the measured $S_{\phi}^{\cdot IV}$ as a function of electron energy from the conduction minimum $E_c$. $D_{it}$ for DHF, O/E, and BW treatments are $2.80\times10^{13}$, $2.71\times10^{12}$, and $4.63\times10^{10}$ states$\cdot$cm$^{-2}\cdot$eV$^{-1}$, respectively. The three lines cross together at a specific point with a barrier height of 0.797 V and a work function value of 4.65 eV, which corresponds to a charge neutrality level (CNL, $\phi_0$). At the CNL, the barrier height is constant, thus being insensitive to the surface cleaning procedures.

Figure 6 shows the Schottky barrier heights for the BW electrodes obtained from the $C-V$ ($\phi_b^{CV}$) and the $I-V$ ($\phi_{b0}^{\cdot IV}$) measurements as a function of $\phi_m$. The inset shows typical plots of $1/C^2$ as a function of the bias voltage, $V$ from Pt, Ni, and Mo electrodes. The straight lines, without detectable bending in any of the lines, indicate that donor atoms distribute uniformly in the SiC epitaxial films. The calculated donor density, $N_D$, in the films is $5\times10^{17}$ cm$^{-3}$. The width of the depletion layer in the films is

TABLE IV. $S_{\phi}$ for each cleaning procedure. $\sigma$ is the standard deviation of $S_{\phi}$. $S_{\phi}^{\cdot}$ indicates $S_{\phi}$ obtained using the ideal barrier height $\phi_{b0}^{\cdot IV}$. The superscripts a and b indicate Ref. 17, 18, and 19–22, respectively.

| | DHF | O/E | BW | Waldrop *et al.*[a] | Porter *et al.*[b] |
|---|---|---|---|---|---|
| $S_{\phi}^{\cdot}$ obtained from $\phi_{b0}^{\cdot IV}$ | 0.215 | 0.739 | 0.994 | | |
| $(\sigma/S_{\phi}^{\cdot})$ | (0.233) | (0.107) | (0.053) | | |
| $S_{\phi}$ obtained from $\langle\phi_{b0}^{IV}\rangle$ | 0.180 | 0.549 | 0.754 | 0.670 | 0.144 |
| $(\sigma/S_{\phi})$ | (0.211) | (0.124) | (0.106) | (0.240) | (0.625) |

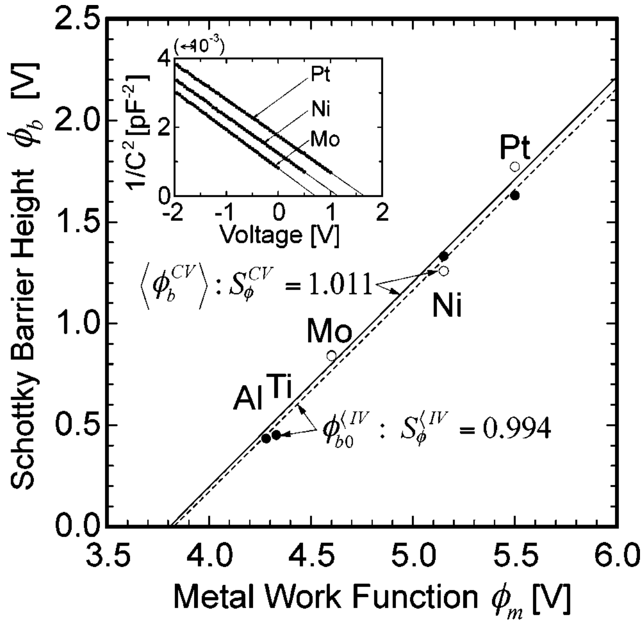


FIG. 6. Schottky barrier heights of BW electrodes measured by $C-V$ ($\phi_b^{CV}$) and $I-V$ ($\phi_{b0}^{\cdot IV}$) methods as a function of $\phi_m$. $S_\phi$ values obtained from $\langle \phi_b^{CV} \rangle$ and $\phi_{b0}^{\cdot IV}$ are 1.011 and 0.994, respectively. The inset shows $1/C^2$ for each metal as a function of the bias voltage $V$. The calculated donor density in the SiC crystal is $5 \times 10^{17}$ cm$^{-3}$.

27 nm. In this doping range, thermionic emission should be the dominant process in interface transport. An important result that can be obtained from this figure is that $\phi_b^{CV}$ is almost equal to $\phi_{b0}^{\cdot IV}$, and thus $S_\phi^{CV}$ with the value of 1.011 obtained from $\langle \phi_b^{CV} \rangle$ is almost the same as $S_\phi^{\cdot IV}$ with 0.994. This indicates that $\langle \phi_b^{CV} \rangle \cong \phi_{b0}^{\cdot IV} > \langle \phi_{b0}^{IV} \rangle$ and $S_\phi^{CV} \cong S_\phi^{\cdot IV} > S_\phi^{IV}$. In other words, the increase in $n$ is the main cause of the barrier–height difference between $C-V$ and $I-V$ measurements in a Schottky barrier with a depletion layer thick enough to assume thermionic emission and a uniform impurity-level profile without any deep level present.

Waldrop *et al.* and Porter *et al.* have studied $\phi_{b0}^{IV}$ of 6H-SiC(0001) epitaxial films for several kinds of metals.[17–22] Our estimations of $S_\phi$ using their barrier heights are listed in Table IV. Waldrop's weak pinning with $S_\phi$ of 0.670 is between the $S_\phi$ values of the O/E and BW electrodes, while Porter's relatively strong pinning of 0.140 is closer to the value of 0.180 of the DHF electrodes. The sample preparation methods in their studies are similar to each other except for an additional cleaning process by $K_2CO_3$ and HCl solution as the last process in the former surface treatment. We propose that the difference in $S_\phi$ originates from the difference in the last process, because the $K_2CO_3$ solution has the effect of etching the SiC surface.[42] The $n$ values for the Ti electrodes in Waldrop's and Porter's works were 1.05 at $\phi_{b0}^{IV} = 0.73$ V and 1.06 at $\phi_{b0}^{IV} = 0.92$ V, respectively.[18,20] These $n$ values are smaller than the values of our Ti electrodes. The reason can be attributed as follows. They heated up their surfaces at 600–700 °C under UHV before metal deposition to remove hydrocarbon contaminants. In general, this kind of *in-situ* cleaning improves $n$. At the same time, it has the effect of desorbing surface terminators such as hydrogen atoms. We heated up our samples only to 200 °C such that we suppressed desorption of the surface terminators. Also, the $K_2CO_3$ process in Waldrop's experiments seems to bring about a decrease in $n$. Actually, the effect of the $K_2CO_3$ process to improve $n$ has already been reported.[42] In Porter's experiments, it is inferred that the strong pinning suppresses the increase in $n$, which is the same behavior as observed in our DHF electrodes. Further, there is statistical uncertainty in their $n$ values because the number of their measured electrodes and mean values of $n$ were not shown in their reports. Although the cleaning procedures of Waldrop's and Porter's experiments are almost the same as ours for the main processes, consisting of thermal oxidation, HF etching, rinse with water, and metal depositions at room temperature under UHV, the $\sigma/S_\phi$ value obtained by Waldrop is about 2 times larger, and that of Porter's is about 5 times larger than the value we saw for the O/E electrodes. Their large values of $\sigma/S_\phi$ may originate from an interfacial chemical reaction. It is likely that the interfacial reaction can occur easily on a surface without terminators, even at room temperature.

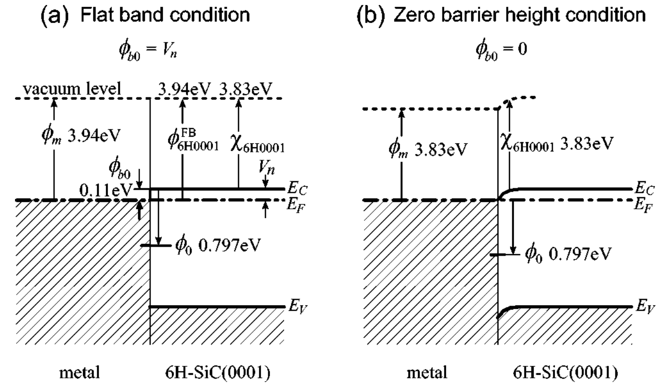


FIG. 7. Specific band diagrams of metal/6H-SiC(0001) interfaces in the Schottky limit condition without interface states. (a) The flat band is formed when $\phi_{bn} = V_n$. (b) When a barrier height for $n$-type is zero, the band in the semiconductor should bend downward so as to realize the zero barrier height at the interface. In conditions (a) and (b), the metal work function, $\phi_m$, should have values satisfying relations of $\phi_m = \chi_S + V_n \equiv \phi_{6H0001}^{FB}$ and $\phi_m = \chi_S$, respectively. Here, $\phi_{6H0001}^{FB}$ is a hypothetical work function whose concept extends to the interface. Since $\chi_{6H0001}$ is 3.83 eV from Fig. 5, $\phi_m$ for (a) and (b) conditions are estimated at 3.94 eV and 3.83 eV, respectively.

In our preliminary experiments using Ti, Mo, and Ni,[43,44] we have estimated values for $\chi_s$ and the flat-band work function $\phi^{FB}$, roughly approximating that $\phi_m$ at $\phi_b^{\cdot IV} = 0$ is the flat-band work function. A more accurate analysis is described as follows. When a semiconductor has a flat-band at the interface as shown in Fig. 7(a), the Schottky barrier height is equal to $V_n$. As calculated earlier, $V_n$ is 0.11 V. From Fig. 5, the work function of a metal at $\phi_{b0}^{\cdot IV} = V_n$ is 3.94 V, which is equal to the flat-band work function $\phi_{6H0001}^{FB}$ of the 6H-SiC(0001) surface. When $\phi_{b0}^{\cdot IV}$ of the pinning–free interface is zero, the work function directly indicates the electron affinity of the 6H-SiC(0001) surface $\chi_{6H0001}$. Thus, the work function intercept of 3.83 V on the $x$-axis in Fig. 5

is $\chi_{6H0001}$. As far as we know, an estimation of the electron affinity from the extrapolation of the experimental Schottky-limit line to the zero barrier height seems to be novel. The band diagram at the zero barrier-height condition is shown in Fig. 7(b). According to an experiment to estimate the conduction band offset at the 6H-SiC(0001)/$SiO_2$ interface using the internal photoemission of electrons,[45] the band offset is 2.95 eV$\pm$0.1 eV. Adding $E_C$=0.9 eV for $SiO_2$[46] to 2.95 eV, an $\chi_{6H0001}$ value of 3.85 V is obtained. The value estimated from the interface band offset shows good consistency with our value obtained from the interfaces with several metals. It should be noted that this estimation of $\chi_{6H0001}$ from the experiment of the SiC/$SiO_2$ interface relies on the assumption that the interface dipole at that interface is negligible. These values are also comparable to a simple classical prediction of 3.7 V, estimated using Pauling's electronegativity.[47]

The three lines in Fig. 5 intersect at a point with a barrier height of 0.797 V and with a work function of 4.65 V. This point is the charge neutrality level (CNL) $\phi_0$[48] experimentally obtained from this graph. The three Mo plots with $\phi_{Mo}$=4.60 V,[32] which are very close to the CNL, have no significant change in barrier height, independent of the surface cleaning procedures. This is because the Fermi levels of Mo and the 6H-SiC(0001) surfaces are almost equal, leading to no charge redistribution. There is a $\phi_0$ value of 1.45 V[48] that is obtained from the previously reported barrier heights by Waldrop[17] and from the Miedema's bulk electronegativity excluding surface effects.[48] This is, however, largely different from our observed value, indicating that $\phi_0$ from the bulk parameter does not necessarily predict a practical CNL value. The details of the CNL discussion have been described in a separate paper.[49]

## IV. SURFACE STRUCTURE TREATED BY BW PROCEDURE

Low-energy electron diffraction (LEED), Auger electron spectroscopy (AES), and x-ray photoemission spectroscopy (XPS) experiments were performed in an UHV system with a base pressure of $1\times10^{-11}$ Torr. The analysis chamber was equipped with a four-grid reverse LEED optics system (VG RVL-900). In AES analyses the electron gun was set at an angle of 60° from the normal of the sample surface. The acceleration energy of the electron beam was 5 keV. The x-ray source used for the XPS analyses was a Mg target with a photon energy of 1253.6 eV. The incident angle of the x-ray beam was at 65° from the surface normal. Spectra of the Auger electrons and the photoelectrons were obtained by a hemispherical analyzer (VG CLAM2) set normal to the sample surface. They were numerically differentiated to obtain $dN(E)/dE$ spectra. The work function of the spectrometer was determined to be 4.38 eV, by subtracting a reported Au $4f_{7/2}$ level of 84.00 eV from the measured Au $4f_{7/2}$ level of a clean Au foil. The samples were typically loaded into the UHV system within 15 min after finishing the final chemical procedure. For comparison, one sample was loaded into the chamber after leaving it in the atmosphere of the experimental room for a few days. The room temperature was set at

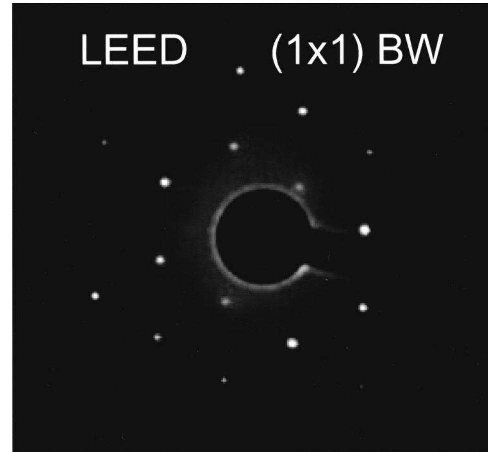


FIG. 8. A $(1\times1)$ LEED pattern observed on a BW-treated 6H-SiC(0001) surface. The primary electron energy is 222 eV.

26.0$\pm$0.1 °C and the typical relative humidity was about 40%. No *in-situ* cleaning was applied to the samples in the AES/XPS system, except the characterization of a surface annealed at 970 °C in UHV.

Scanning tunneling microscopy (STM) measurements were carried out at room temperature in an UHV system (UNISOKU USM-501), with a base pressure of $2\times10^{-11}$ Torr. In the STM analysis, a sample just after BW immersion was introduced into a glove box with a nitrogen atmosphere, which we used to protect the sample surface from contamination and oxidation. The oxygen density in the glove box was less than 2 ppm, and the number of particles of size $\geqslant$0.1 $\mu$m per cubic foot was zero. The sample was loaded into the STM system under the clean atmosphere using a stainless-steel transfer box that transferred the sample from the glove box to the STM system, which was remote from the glove box. In order to desorb water molecules from the sample surface, the sample was annealed at 400 °C for 3 hours at a maximum pressure of $2\times10^{-9}$ Torr. In the literature describing hydrogen termination and desorption on 3C-SiC(001) surfaces, a temperature over 700 °C is needed for hydrogen desorption.[50] Therefore, the temperature of 400 °C that we used here is much lower than the critical temperature.

As experimental results, we first mention the wetting characteristics of the sample surfaces. In our visual inspection, as-received epitaxial samples and DHF samples were hydrophobic while O/E and BW samples show hydrophilic. These behaviors are in high contrast to that of Si surfaces in the HF rinsing process. Since the O/E and BW treatments include the HF rinsing process but their samples are hydrophilic, it is intuitively inferred that the O/E and BW surfaces tend to be covered with some oxidized species whose structure is different from amorphous $SiO_x$. From AES and XPS analyses, no carburized species that often shows hydrophilic nature was found. These results are the same as experimental results of wet chemical processing using nonepitaxial SiC wafers in a recent literature.[51] In this paper, we mainly focus our description on surface characterizations into those of the BW surface that generates the pinning–free interface after

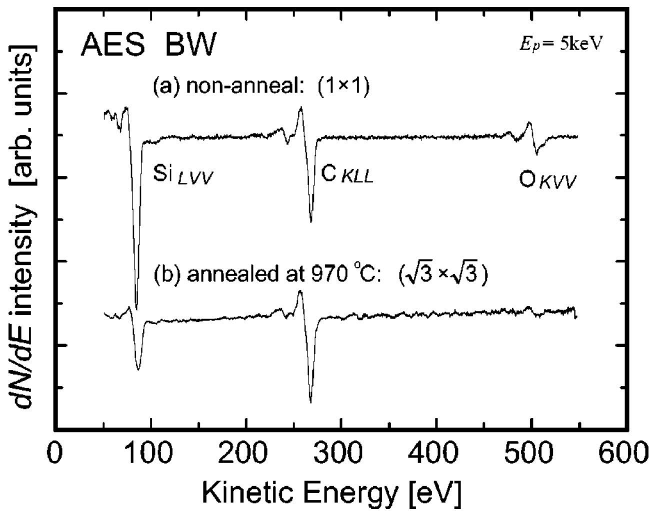


FIG. 9. Survey spectra of $dN(E)/dE$ for BW samples (a) without *in-situ* anneal and (b) with an UHV anneal at 970 °C. The primary electron energy $E_p$ is 5 keV.

the metal depositions. Some results from DHF and O/E surfaces are mentioned as a comparison.

In LEED observations, no spots were observed on a DHF sample, indicating a disordered structure of the surface. An O/E sample showed an ordered $(1\times1)$ pattern, which is the same result as previous reports.[17,20,24,51] This indicates that the O/E process removed the disordered surface layer. Figure 8 shows the $(1\times1)$ LEED pattern observed on a BW-treated surface. No detectable difference was found between the O/E-treated surface and the BW one from the LEED observations.

Figure 9(a) shows a survey spectrum of $dN(E)/dE$ for a BW sample. Dominant Si $LVV$ and C $KLL$ peaks were observed as well as the detection of an O $KLL$ peak. The relative oxygen concentration of the BW surface calculated us-

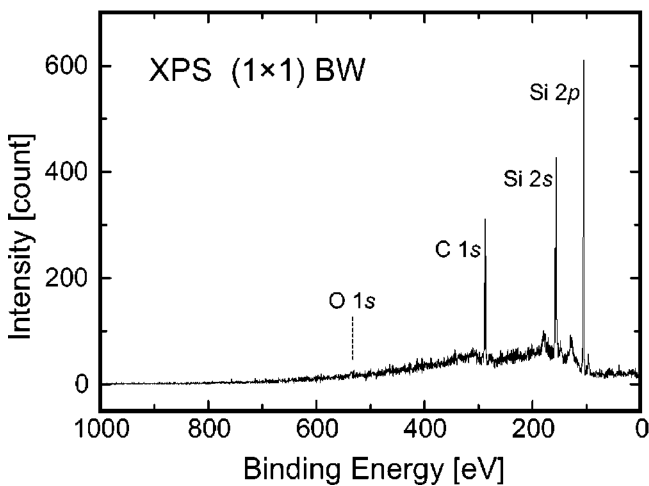


FIG. 10. XPS spectrum of a BW-treated surface loaded into the chamber immediately after the treatment, within 5 min and measured within 2 hours. No significant peaks related to oxygen are observed. Note that the spectrum was taken from the as-loaded sample without *in-situ* cleaning.

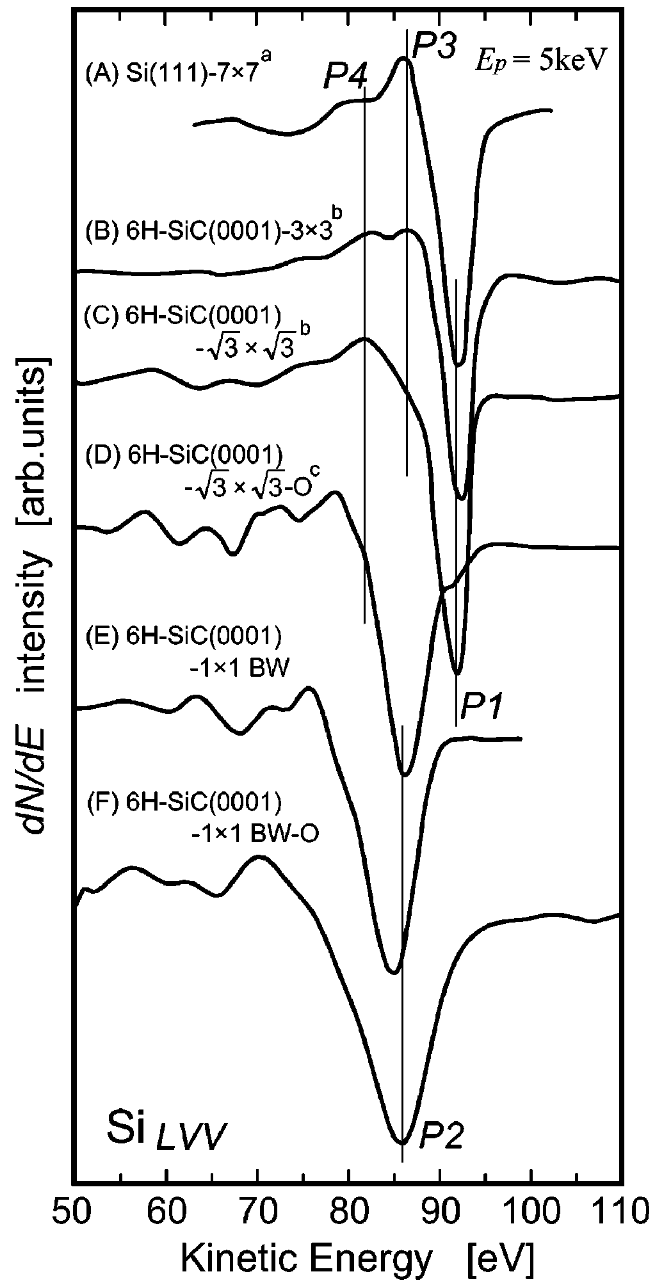


FIG. 11. Si $LVV$ AES line shapes of (A) the Si(111)-$7\times7$ surface, (B) the 6H-SiC(0001)-$3\times3$ surface, (C) the 6H-SiC(0001)-$\sqrt{3}\times\sqrt{3}$ surface, (D) the oxygen-adsorbed 6H-SiC(0001)-$\sqrt{3}\times\sqrt{3}$-O surface, (E) the 6H-SiC(0001)-$1\times1$ BW surface. Spectrum (F) is a BW sample exposed in air for a few days. No *in-situ* anneals were applied for (E) and (F). The superscripts a, b, and c indicate Ref. 55, Ref. 56, and Ref. 57, respectively.

ing relative sensitivity factors[52] is less than 5%. Oxygen is known to remain on the 6H-SiC(0001) surface even after dipping it in HF solution.[17,20,24,51,53] This suggests that oxygen atoms adsorb in a different form to $SiO_x$ that can be removed completely by HF solution, as was mentioned by Elsbergen *et al.*[53] Oxygen concentrations reported by Waldrop *et al.*,[17] King *et al.*,[51] Elsbergen *et al.*,[53] and Porter *et al.*[20] are 75%, 75%, 60%, and 9.3%, respectively. A de-

tectable but faint O *KVV* peak was observed in the report by Starke *et al.*[24] An increase in oxygen concentration on 6H-SiC surfaces under an oxygen environment was also reported.[54] We loaded the SiC sample whose AES spectra are shown in Figs. 9(a) and 9(b) into the vacuum chamber soon after the chemical treatment, but the AES spectra were measured one day after sample loading. A sample loaded into the chamber immediately just after the treatments, (within 5 min), and an XPS measurement within 2 hours had no remarkable oxygen, as shown in Fig. 10. For a BW sample left in an air environment for a few days, a large surface oxygen content of 75% was detected. These results indicate that the oxygen adsorption on the 6H-SiC(0001) surface depends strongly on the surface cleaning procedures and the exposure condition to the environment. Typically, our BW samples had residual surface oxygen levels of less than 5%.

Spectrum (E) in Fig. 11 shows a Si *LVV* peak of the $(1\times1)$ BW-treated sample indicated in Fig. 9(a). Spectrum (F) is the BW sample exposed in air for a few days. Those of the Si(111)-$(7\times7)$ surface (A),[55] the 6H-SiC(0001)-$(3\times3)$ surface (B),[56] the 6H-SiC(0001)-$(\sqrt{3}\times\sqrt{3})$ surface (C),[56] and the oxygen-adsorbed 6H-SiC(0001)-$(\sqrt{3}\times\sqrt{3})$ surface (D)[57] are also depicted in Fig. 11 as references. Surface (D) was formed by exposing surface (C) to an oxygen atmosphere. Prominent negative peaks in spectra (A)–(C) are located at the same position $P1$ of 92 eV. For spectra (D)–(F) peak $P1$ largely shifts to peak $P2$ at 85-86 eV. Significant features common to the surfaces of group (A)–(C) are the presence of dangling bonds and lack of oxygen, since they are formed by *in-situ* UHV cleaning and a high temperature anneal. A surface state in the band gap has been found for the $(\sqrt{3}\times\sqrt{3})$ surface in experiments of valence band photoemission[58] and scanning tunneling spectroscopy (STS).[59] Surface states for the $(3\times3)$ surface are also supported by a theoretical calculation.[60] According to structural models for the $(3\times3)$ surface and the $(\sqrt{3}\times\sqrt{3})$ surface, the $(3\times3)$ surface has a majority of Si atoms on the Si–C topmost bilayer[61] and the $(\sqrt{3}\times\sqrt{3})$ surface has one monolayer of Si adatoms at the $T_4$ site on the topmost Si–C bilayer.[62] This indicates that another feature of the $(3\times3)$ and the $(\sqrt{3}\times\sqrt{3})$ surfaces is the presence of Si–Si bonds.

In our STS experiments for a BW surface formed under the same cleaning condition as surface (E), no perceptible signal was observed in the whole range of the 6H-SiC band gap. This indicates that the BW surface has few surface states, with a density of at least less than the detection limit of roughly $10^{13}$ $\mathrm{cm}^{-2}$ in our STS system. Thus, one of the important features of group (D)–(F) is the absence of surface states or surface passivation. Since the oxygen concentration on surface (E) is $<5\%$, the presence of oxygen has a minor effect in the AES spectra shapes for the passivated group.

Two distinct positive peaks, $P3$ and $P4$, in the energy range of 80–90 eV, are observed in spectra (A)–(C). The height of $P3$ increases as we increase the surface Si concentration from (C) to (A). $P4$ is observed also in spectrum (D) as a shoulder, but is not detected in spectra (E) and (F). We formed the passivated $(1\times1)$ surfaces (E) and (F) by a wet chemical procedure that did not supply Si atoms onto the surfaces, which should then form a surface without the Si–Si bond. Thus, the origin of $P4$ can be assigned to the Si–Si bond. From the above interpretation, it was found that the $(1\times1)$ BW surface is characterized by having no surface states, no Si–Si bond, and a small amount of residual oxygen.

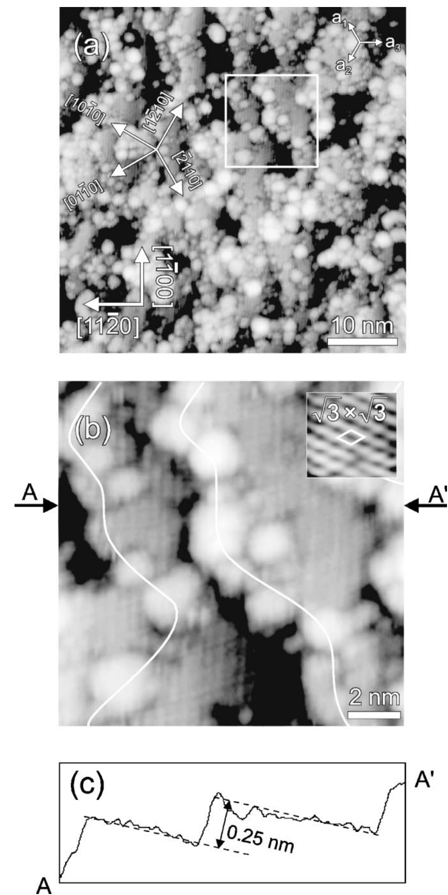


FIG. 12. (a) A topographic STM image of a BW surface annealed *in situ* at 970 °C. The image area is $50\times50$ nm. The sample bias voltage and the tunneling current are −2.41 V and 0.35 nA, respectively. (b) A magnified image of the area indicated by the white frame in (a). White lines trace edges of atomic steps. The terraces have a $\sqrt{3}\times\sqrt{3}$ reconstruction as shown in the inset. (c) A cross-sectional topography of line A-A′ in (b). The measured step height of 0.25 nm corresponds to the bilayer step height on the 6H-SiC(0001) surface.

For a C *KLL* spectrum, it is known that the shape and position are insensitive to surface reconstructions.[53,57,63] As we also expected, in our observation, the C *KLL* spectrum of surface (E) exhibited little difference from that of the $(1\times1)$ surface reported previously.[53]

After annealing the BW-treated surface (E) at 970 °C for 2 min in UHV, we obtained a $\sqrt{3}\times\sqrt{3}$ pattern in LEED analysis. On the surface, we still observed half the oxygen concentration that we had observed before the anneal, as shown in Fig. 9(b). On the contrary, in typical cleaning procedures similar to the DHF and O/E treatments, it is well known that residual oxygen desorbs completely from a typical HF-prepared surface during an UHV heat treatment at ~900 °C on the 6H-SiC(0001) surface.[53,64] This is owing to the etching effect of oxygen, where oxygen is in equilibrium in the

desorption mode during a high temperature UHV anneal.[63] Thus, the residual oxygen after the anneal at 970 °C in this experiment suggests stronger chemical bonding of the oxygen atoms with the BW surface.

Our STM observation for a BW sample gave us an unclear atomic image. This might be due to water adsorption onto the measurement tip from the sample surface. Instead, we observed clear $(\sqrt{3}\times\sqrt{3})$ atomic images from annealed BW samples at 970 °C. These images help us to analyze the atomic step structure. Also, the analysis of the $(\sqrt{3}\times\sqrt{3})$ surface provides us useful information on electronic and structural information for deeper understanding of the $(1\times1)$ BW surface. As for STS experiment without tip scanning, nonannealed BW surfaces were measured at room temperature.

Figure 12(a) is a topographic STM image of the annealed surface with an area of $50\times50$ nm. The sample bias voltage and the tunneling current are $-2.41$ V and 0.35 nA, respectively. Figure 12(b) shows a magnified image of the area indicated by the white square in Fig. 12(a). A periodic atomic arrangement was found on terraces. A further magnified image with atomic resolution is shown in the inset of Fig. 12(b). The white rhombus in the inset corresponds to the unit cell of the 6H-SiC(0001)-$(\sqrt{3}\times\sqrt{3})$ reconstruction, with a side of 0.5336 nm. This reconstruction is consistent with the $(\sqrt{3}\times\sqrt{3})$ LEED pattern. Since we supplied no Si atoms onto the $(1\times1)$ BW surface and the resultant $(\sqrt{3}\times\sqrt{3})$ surface, it is probable that the $(\sqrt{3}\times\sqrt{3})$ surface has no extra Si on the Si-terminated surface. For a $(\sqrt{3}\times\sqrt{3})$ surface formed by a common cleaning procedure with a Si molecular flux in UHV, the $T_4$-site model with Si adatoms is proposed.[62] This implies that the surface structure of the $(\sqrt{3}\times\sqrt{3})$ formed from the terminated $(1\times1)$ surface by carrying out the UHV anneal should be different from the reconstruction with the Si adatoms. Actually, the observed filled-state atomic image in STM exhibits a rhombus mesh that is totally different from the filled-state image of the adatom surface consisting of round protrusions.[65] A possible structure is that of a Si trimer structure, without any Si adatoms on the topmost Si layer. For this surface with lower Si coverage, extensive studies are needed to determine the true atomic structure. Figure 12(c) shows the cross-sectional topography of line A-A′ in Fig. 12(b). The measured step height of 0.25 nm corresponds to the bilayer step height of 0.252 nm [= (the vertical lattice constant $c$)/6] on the 6H-SiC(0001) surface. The step-edge lines tend to have zigzag features composed of lines along the $[1\bar{2}10]$ and $[\bar{2}110]$ directions. This geometric shape is the same as that seen on the UHV-annealed clean 6H-SiC(0001) surfaces tilted toward the same $[11\bar{2}0]$ direction.[66,67] The average width of terraces in the $[11\bar{2}0]$ direction is measured to be $\sim$5 nm, which agrees with the width of 4.12 nm estimated from the macroscopic off-angle of 3.5° in this direction. This indicates no vertical undulations of the terraces in the $[11\bar{2}0]$ direction. Further, no step bunching was observed as far as our interpretation of observed topographic images could establish. From the LEED observation, no long range ordering was observed as shown in Fig. 8. This indicates that the terrace widths have some fluctuation, which is consistent with fluctuated terrace widths observed in Fig. 12(a).

One of the most important features seen in the STM images is that the adsorbates at the step edges appeared as white large protrusions. It should be noted that this image was observed after heat treatment at 970 °C. Since this surface has Si and C atoms as its main constituent atoms, and only a small concentration of oxygen atoms, it is reasonable to ascribe the protrusions to the observed residual oxygen. The coverage of the white protrusions in Fig. 12(b) is $\sim$15%, which is larger than the oxygen concentration of $<$5% estimated from the AES peak ratio. This discrepancy may come from a low spatial resolution at a step edge in the STM measurements. Generally, the resolution becomes lower at a step edge and at an adsorbate, where the height changes steeply. The resolution of such a steep slope depends on the radius of the tip apex, not on the true sample slope. In the case of a step edge with adsorbates, the size of the protrusion tends to be emphasized in an STM scan.

Here, we estimate the number of atoms at the step edges. From the off-angle of 3.5° in the $[11\bar{2}0]$ direction, the average terrace width in the $[11\bar{2}0]$ direction is 4.12 nm. This is converted to a width of $4.12\times\cos30°=3.57$ nm in the $[01\bar{1}0]$ or $[10\bar{1}0]$ direction. The number of step-edge lines per unit length in the $[01\bar{1}0]$ or $[10\bar{1}0]$ direction is $1/(3.57\text{ nm})=2.80\times10^8\text{ m}^{-1}$. From the lattice parameter $a$ of 0.30806 nm for the 6H-SiC(0001) crystal, the density of surface atoms along the step edges is $1/a=3.2461\times10^9\text{ m}^{-1}$. Thus, the total number of step edge atoms is $(2.80\times10^8\text{ m}^{-1})\times(3.246\times10^9\text{ m}^{-1})=9.09\times10^{13}\text{ cm}^{-2}$.

On a 6H-SiC(0001) surface tilted in the $[11\bar{2}0]$ direction, the number of dangling bonds and terminated bonds per one step-edge atom in the $[01\bar{1}0]$ and $[10\bar{1}0]$ direction changes alternately between one bond and two bonds every three bilayers. This is because the hexagonal stack (eclipse configuration) appears once in three bilayers in the 6H-SiC crystal, which has a layer stacking sequence of ABCACB... in the [0001] direction. Along a zigzag line, the bond number is one in the span of a $[01\bar{1}0]$ step, while it is two in the span of the other $[10\bar{1}0]$ step. These numbers are exclusive to each of the two step directions in a connecting step edge line. Thus, the average bond number is 1.5. The calculated density of step edge bonds is $(9.09\times10^{13}\text{ cm}^{-2})\times1.5=1.36\times10^{14}\text{ cm}^{-2}$. This value is sufficient to pin the surface Fermi level[68] even under conditions of perfect termination of the terraces, when all the bonds at the step edges are dangling bonds. In the actual BW interface, the Fermi level is free from pinning, indicating that almost all atoms on the step edges at the interfaces are terminated.

We focus our discussion on the terrace termination of the $(1\times1)$ BW-treated 6H-SiC(0001) surface. From the interpretation above, the surface is characterized by oxygen termination at the step edges, with no dangling bonds on the $(1\times1)$ reconstruction, and the detection of dominant Si and C concentrations with only a small concentration of oxygen. These features indicate that the most probable terminator of the top-most Si atoms on the terraces is hydrogen. It is well

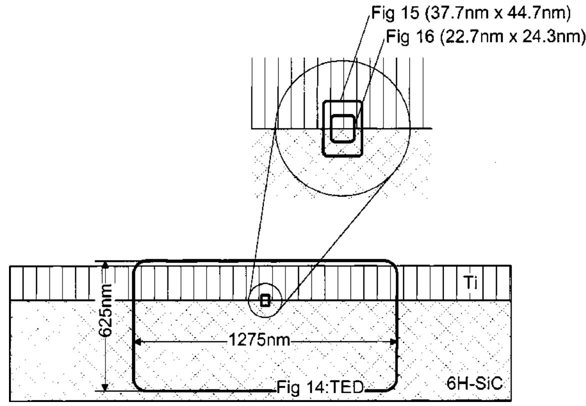


FIG. 13. A schematic diagram of cross sections of Ti/6H-SiC samples used for TEM/TED measurements. The observed areas are depicted.

known that the boiling water dip treatment terminates the Si(111) surface by the monohydride.[25,26] This behavior of boiling water is consistent with hydrogen termination on the 6H-SiC(0001) surface. On a 6H-SiC(0001) surface annealed in a $H_2$ atmosphere at 1000 °C, a sharp absorption peak originating from the vertical Si–H vibration was observed by infrared attenuated total reflection spectroscopy (ATR),[69] which evidenced that the hydrogen termination is real on the SiC(0001) surface. The terminators of the 6H-SiC(0001) surface dipped in buffered $NH_4F$ solution were characterized by Stark *et al.* using high-resolution electron energy loss spectroscopy (HREELS).[24] The O–H stretching mode of hydroxyl species with a small concentration of oxygen was detected. This suggests that another possible structure is OH group termination as a minor contribution on the terraces and at the step edges. The degree of surface band bending before metal deposition was evaluated from our XPS spectrum. The energy difference between the carbon 1$s$ core level $E_{C1s}$ and the valence band maximum $E_V$ for the 6H-SiC(0001) surface, which is independent of the surface band bending, has been reported to be 281.26 eV.[18] Using this value, the surface potential barrier height $\phi^s_{bn}$ for $n$-type is expressed as[20]

$$q\phi^s_{bn} = [(E_{C1s} - E_V) + E_G] - E_{C1s}. \quad (8)$$

Substituting the value of 2.86 eV for $E_G$ of the 6H-SiC crystal,[70] Eq. (8) is rewritten as $q\phi^s_{bn} = 284.12 - E_{C1s}$. We obtained the value of 283.93 eV for $E_{C1s}$ from the BW-treated surface, leading to $\phi^s_{bn}$ of 0.19±0.10 eV. The value 0.19 eV corresponds to a band bending of 0.08 eV, since $V_n$ is 0.11 V. The density of the surface states required to generate this small surface barrier height of 0.19 eV is $1.1 \times 10^{12}$ states·cm$^{-2}$·eV$^{-1}$.[49] This coincides with no surface states being detected in the STS measurement. Although this potential barrier is much smaller than the band gap, the band of the BW-treated surface is not perfectly flat. Such an imperfect flattening of the surface band is improved at the interface formed with the metals, as we observed for the Schottky limit with $D_{it}$ of $1.12 \times 10^{11}$ states·cm$^{-2}$·eV$^{-1}$. There are two important features found in these results on the state densities and the band bendings. Bardeen has already

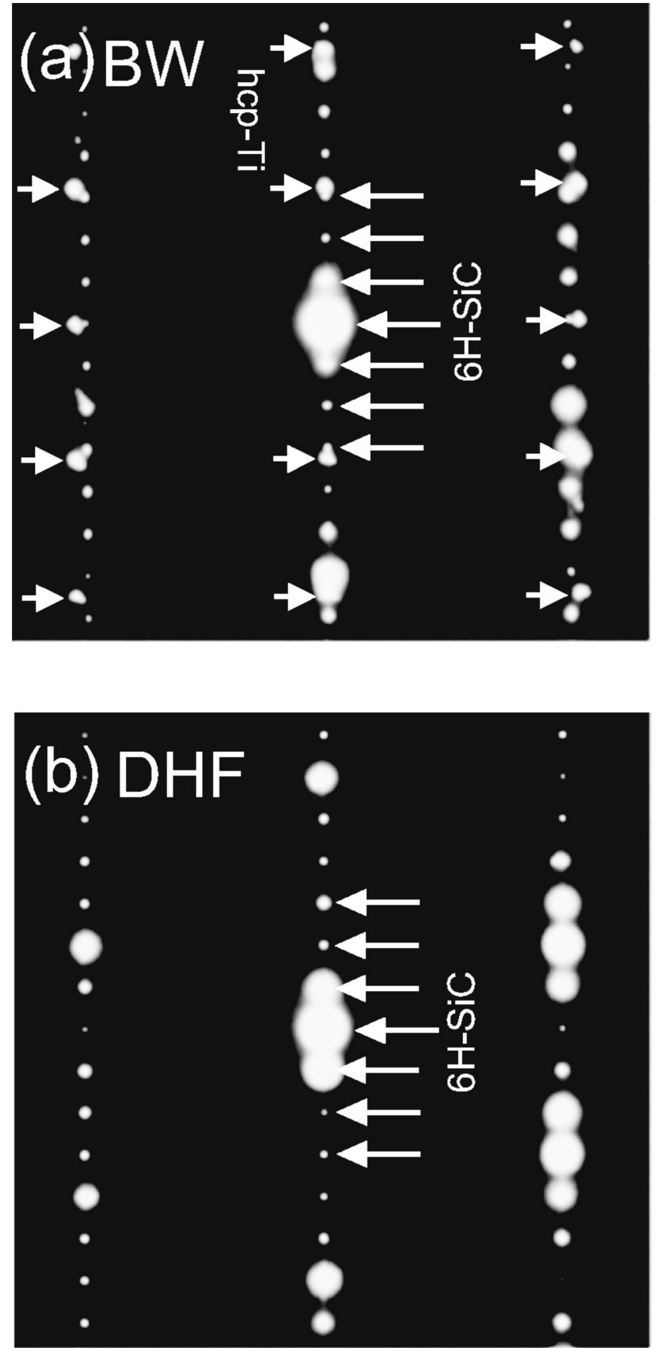


FIG. 14. TED patterns of (a) BW-treated and (b) DHF-treated Ti/6H-SiC interfaces. Diffraction spots indicating the 6H-SiC crystal were observed from both interfaces. Additional spots corresponding to the hcp-Ti structure were observed only from the BW-treated interface.

pointed out that the density of the surface states needed to pin the Fermi level is one order less than that required at the interface, indicating an easier pinning trend of the surface.[68] Thus, even if we assume that the surface states of $1.1 \times 10^{12}$ states·cm$^{-2}$·eV$^{-1}$ is preserved after the interface formation, the density would have a much less effect to bend the interface band, forming an almost unpinned interface. The actual interface, however, has $1.12 \times 10^{11}$ states·cm$^{-2}$

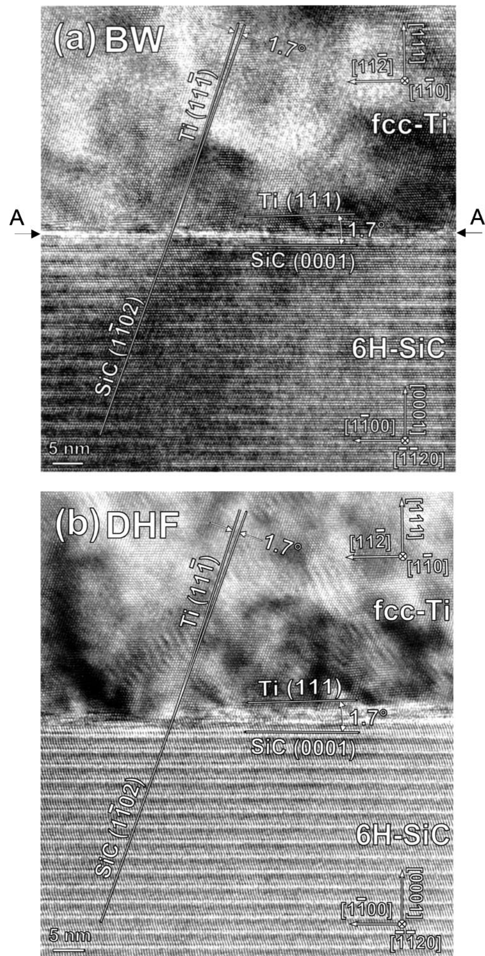


FIG. 15. TEM images of (a) BW-treated and (b) DHF-treated Ti/6H-SiC interfaces. The Ti layers on both BW- and DHF-treated SiC surfaces have a face-centered cubic crystal structure. The face angle between the Ti(111) and the SiC(0001) faces is 1.7°. The face angle between the Ti($11\bar{1}$) and the SiC($1\bar{1}02$) faces is also 1.7°.

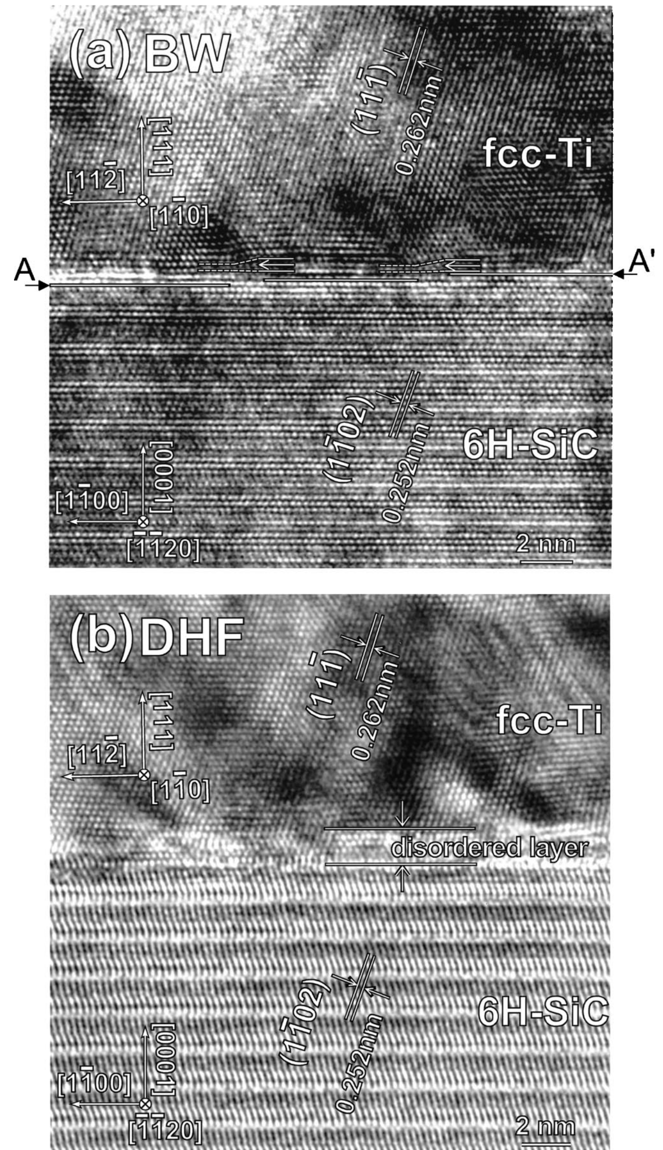


FIG. 16. Magnified TEM images of (a) the BW-treated and (b) DHF-treated Ti/6H-SiC interfaces. In the Ti/BW-treated SiC interface shown in (a) no dislocations were observed right at the interface, while half planes were inserted inside the Ti film few ML apart from the interface as depicted by white arrows in (a). In the Ti/DHF-treated SiC interfaces shown in (b) there is a disordered layer ~2 nm in thickness, where disorder exceeds its degree enough to identify individual atomic layers but the degree is much less than amorphous structure.

$\cdot \mathrm{eV}^{-1}$, which is one order lower density than that of the surface. This indicates that the almost residual surface states were passivated by the metal depositions. From the strong linearity of the BW plots in Fig. 5, it is found that this state passivation ratio of $D_{it}/D_s$ is constant independent of the deposited metals.

## V. INTERFACE STRUCTURE

Atomic structures of Ti/SiC interfaces formed by the pinning–free BW- and the pinned DHF-treatments were characterized by high-resolution transmission electron microscopy (HRTEM). The surface cleaning procedures used were exactly the same as those used for the samples that we prepared for electrical measurements. Titanium films, 120 nm in thickness, were deposited on the samples at room temperature after outgassing of the samples at 200 °C under UHV. The deposition rate was 2 nm/min.

Two Ti/SiC samples were glued together by epoxy resin with the titanium surfaces facing each other. This face-to-face sample was cut, polished, dimpled, and $\mathrm{Ar}^{+}$ ion-beam sputtered sequentially. An amorphous carbon layer was deposited to prevent the sample from incorporating surface contaminants during TEM observations. The observation direction was along the $[\overline{1}120]_{\text{6H-SiC}}$ crystal axis. In the epitaxial 6H-SiC(0001) films used for the electric and surface characterizations with an off-cut angle of 3.5° toward the $[11\bar{2}0]_{\text{6H-SiC}}$ axis, the atomic steps toward the $[11\bar{2}0]_{\text{6H-SiC}}$ axis resulted in cross-sectional interface images which were dull, and apparently insufficient to obtain the lattice resolution. Further, the resolution of cross-sectional image observation toward the $[1\bar{1}00]_{\text{6H-SiC}}$ axis is worth than that toward

the $[\overline{11}20]_{6H\text{-}SiC}$ axis. Thus, nonepitaxial 6H-SiC(0001) substrates with on-axis surfaces, which were grown by the modified-Lely method, were mainly used for the TEM characterizations. TEM images and diffraction patterns shown in this report were taken from the on-axis samples. Since we focus our TEM analyses into atomic-scale interface structures, on-axis samples are sufficiently useful for an investigation of the interface systems. The TEM system was a JEOL JEM-400EX, with an acceleration voltage of 300 kV.

Figure 13 shows schematics of the TEM observation areas for the BW-treated and DHF-treated samples. The wider observation area of 1275 nm×625 nm contains the whole titanium film in its deposition direction. From a cross-sectional image of this area, the thickness of the Ti film was found to be uniform, and evaluated as being ~120 nm. Figures 14(a) and 14(b) show transmission electron diffraction (TED) patterns of the BW-treated and DHF-treated interfaces in the observation area, respectively. Figures 15(a) and 15(b) show cross-sectional images with an observation area of 37.7 nm ×44.7 nm, as in Fig. 13. The magnified images shown in Figs. 15(a) and 15(b) are Figs. 16(a) and 16(b) with an observation area of 22.7 nm×24.3 nm.

The BW interface has sufficient interface abruptness to identify the interface position, which was determined as being the position where the periodical 6H-SiC lattice ends. This position is indicated by the white line A-A′ in Fig. 16(a). The abrupt interface indicates that there is no formation of silicide and carbide phases. The SiC and the Ti layers have a commensurate interface arrangement, and no dislocations are observed at the interface. Some edge dislocations occur within the Ti film, 2 to 3 monolayers away from the interface, as indicated by the white arrows.

All steps observed at the interface of the BW-treated sample were single bilayers, as shown along the line A-A′ in Fig. 16(a). The direction of the steps is towards $[1\bar{1}00]_{6H\text{-}SiC}$. The steps observed at the interface along the $[1\bar{1}00]_{6H\text{-}SiC}$ direction were formed in the process of wafer cutting, dicing, or during the sample preparation.

On the other hand, the DHF-treated sample had a disordered region, as shown in Fig. 16(b). The thickness of the disordered region is ~2 nm. The Ti film has a periodical structure above the disordered region. Dislocations were observed in the periodical layer. Even in the disordered layer the lattice is resolved, suggesting the degree of disorder is relatively small. As mentioned in the previous section, no LEED spot was observed from the DHF sample, suggesting that a part of the disordered region belongs to the SiC substrate, and the Ti/SiC interface is present in the disordered region. As clearly observed, the abrupt interface forms on the flat and well-ordered BW surface while the interface has the disordered layer on the DHF surface with the disordered degree of no periodical surface lattice.

The nearest plane spacing parallel to the interface in the Ti film in Fig. 16(a) is 0.219 nm. This is clearly different from the tabulated value of 0.234 nm for the (0002) planes in the most stable Ti hexagonal close packed (hcp) structure. Also, the (011) plane that was observed as being a typical plane in the cross-sectional TEM investigation of the hcp-Ti layer on 6H-SiC(0001) substrates, which is discussed in Ref. 20, is not observed in the BW and DHF interfaces in Fig. 16. The lattice image in Fig. 16 is also inconsistent with the known body-centered cubic (bcc) structure of Ti. From a detailed analysis of the BW interface using cross-sectional TEM images and TED patterns, we have identified that the Ti structure in Fig. 16 is a face-centered cubic (fcc) structure, with a lattice constant $a_{fcc\text{-}Ti}$ of 0.438 nm.[71] The crystallographic relationships between the fcc-Ti layer and the 6H-SiC crystal at this interface are $(111)_{fcc\text{-}Ti}//(0001)_{6H\text{-}SiC}$ and $[\bar{1}10]_{fcc\text{-}Ti}//[11\bar{2}0]_{6H\text{-}SiC}$. Misfit parameters between $(11\bar{1})_{fcc\text{-}Ti}$ and $(1\bar{1}02)_{6H\text{-}SiC}$ planes and between $(002)_{fcc\text{-}Ti}$ and $(\bar{1}104)_{6H\text{-}SiC}$ planes calculated using $a_{fcc\text{-}Ti}$ are 0.52% and 0.48%, respectively. In this calculation, the lattice constants 0.30806 nm for $a$ and 1.51173 nm for $c$ for the 6H-SiC(0001) crystal were used.[41]

It has been reported that ultra-thin fcc-Ti layers were formed on Al(011) and Al(001) surfaces, where the thickness of the fcc-Ti films were less than 1 nm.[72,73] In our study, fcc-Ti films with a thickness of over 20 nm were formed as shown in Figs. 15(a) and 15(b). This is the first demonstration of a thick fcc-Ti film. The lattice mismatch of ~0.5% mentioned above between the fcc-Ti and 6H-SiC crystals is much smaller than the value of 2.34% between the fcc-Ti and Al crystals. This seems to be the cause of the formation of the thick layer.

Diffraction spots corresponding to the 6H-SiC crystal were observed from the BW and DHF samples, as indicated by the long white arrows in Figs. 14(a) and 14(b). Additional spots were found as indicated by the short white arrows in Fig. 14(a). The lattice constant obtained from the width of periodical spots is 2.95 Å, which is consistent with the hcp-Ti structure. From the TED pattern, it is found that titanium has the fcc structure near the interface region and changes into the hcp structure toward the surface region. The structural change depends strongly on the conditions used for the titanium deposition. When we deposited Ti at a deposition rate of 1 nm/min, i.e., two times slower than the rate for the samples of Fig. 16, the crystal structure of the titanium film was fcc throughout the 80 nm of Ti film that we deposited.[71]

Porter *et al.* reported that a Ti crystal deposited on a 6H-SiC(0001) surface has the hcp structure.[20] Although there is no significant difference in sample preparation procedures between their experiments and ours, a noticeable difference occurs in the surface termination conditions. They deposited titanium at room temperature after annealing their SiC surface at 700 °C under UHV. At such an elevated temperature, hydrogen atoms on the SiC surface desorb, resulting in a surface without any terminators. Since the anneal temperature in UHV was 200 °C in our sample preparation regime, hydrogen atoms terminate until the metal deposition. The commensurate arrangement of the Ti layer and the SiC layer at the BW interface against the lattice mismatch of ~0.5% suggests that the hydrogen terminator desorbs during the initial stages of Ti deposition. The differences in hydrogen desorption *before* and *during* the Ti depositions generate the difference in the heat of interface formation. On the nonter-

minated surface the chemical bonding between Ti atoms and the SiC substrate generates heat of formation, thereby heating itself. On the terminated surface, the terminator can be replaced by the Ti atoms, resulting in the reduction of heat of interface formation. Also, the terminated surface seems to enhance the surface migration of the Ti atoms. Actually, the thickness fluctuation of the Ti film for the BW procedure is considerably smaller, with a value of around $\pm 1.5\%$.

The commensurate Ti arrangement, without any dislocations near the interface against the $\sim 0.5\%$ lattice mismatch generates strain inside the Ti layer. This strain causes edge dislocations inside the Ti layer. The nearest edge dislocations to the interface are indicated by the white arrows in Fig. 16(a). These dislocations form extra half planes. Above these dislocations, further dislocations (not indicated) occur to release the residual strain. The generation of a few half planes results in the tilting of the Ti layer. In both the BW and DHF interfaces, the $[111]_{\text{fcc-Ti}}$ direction was tilted by $1.7°$ in the $(11\bar{2}0)_{\text{6H-SiC}}$ plane with respect to the $[0001]_{\text{6H-SiC}}$ direction, as shown in Figs. 15(a) and 15(b). The face angle between the Ti$(11\bar{1})$ and the SiC $(1\bar{1}02)$ faces for the BW and DHF specimen interfaces was also $1.7°$. When titanium was deposited on the BW-treated SiC surface at the low deposition rate of 1 nm/min, the tilt angle was raised to $3.5°$. This indicates that the tilt angle does not depend on the SiC surface conditions, but depends on the metal deposition rate. The number of half planes determines the tilt angle of the crystal axis of the titanium film with respect to the SiC crystal. A detailed analysis on the Ti/6H-SiC(0001) interface is reported in Ref. 71. Also, in the 6H-SiC(0001) epitaxial samples with an off-cut angle of $3.5°$ toward the $[11\bar{2}0]_{\text{6H-SiC}}$ axis, we infer that the fcc-Ti layer tilts toward the same direction. This is because these two tilt angles toward the $[1\bar{1}00]_{\text{6H-SiC}}$ direction for the Ti rotation and the $[11\bar{2}0]_{\text{6H-SiC}}$ axis for this off-cut angle are perpendicular or geometrically independent.

In this section, TEM measurements were carried out only for the Ti/SiC interfaces. As observed in the cross-sectional images, an abrupt interface formed, even for the titanium atoms with their highly reactive nature. Considering both the low $D_{it}$ and the good $\phi_m$ linearity of the BW interfaces, as shown in Fig. 5 and the lower reactivity of the other metals used, abrupt interfaces, similar to the Ti/SiC interface, should be formed for the other metals.

## VI. DISCUSSION

What should be discussed first is the origin of the interface states observed in the metal/6H-SiC(0001) interfaces. We found several critical features that the interface states are related to interface disorder. First of all, the CNL $(=\phi_0)$[74] we observed was 0.797 eV, which is totally different from 1.45 eV predicted as $\phi_0$ inherent in MIGS.[48] Thus, the large difference of $\phi_0$ indicates that the origins of the MIGS and the observed states are different. Also, the observed $D_{it}$ strongly depends on the surface preparation procedures, which is inconsistent with the nature of MIGS. Second, the strong linearity in the relations between $\phi_m$ and $\phi_{b0}^{\cdot IV}$ observed in Fig. 5 directly indicates that $D_{it}$ is constant in each surface preparation procedure. This is also depicted as constant $D_{it}$ in the inset in the figure. This broad distribution of $D_{it}$ in the band gap suggests that there are various kinds of local atomic structures. Since the values of $D_{it}$ are much lower than the areal density of atoms and we have observed lattice images at the interfaces by TEM, the various kinds of local atomic structures are distributed sparsely in the SiC lattice which has a periodical atomic arrangement. Note that the $D_{it}$ value of $4.63\times 10^{10}$ states$\cdot$cm$^{-2}\cdot$eV$^{-1}$ for the BW interface corresponds to the inter-states distance of $\sim 50$ nm, which is much larger than the distance of several nanometers necessary to form a band only by the states. This is a kind of disorder whose degree is much smaller than that of topological disorder like amorphous. Although this is one of weak class of disorder in the lattice, the density of interface states caused by this disorder is sufficient to pin the Fermi level, especially for DHF treatment. It should be noted that a specific defect structure to form a local defect center in the band gap is excluded because of the energetically broad feature. Third, no LEED pattern was found on the DHF surface, indicating that the surface is disordered in atomic scale. The observations of ordered $(1\times 1)$ patterns in O/E and BW surfaces correspond to the improvement of the perfectivities in surface atomic arrangements. Last, a disordered layer with the thickness of $\sim 2$ nm in the DHF interface was clearly observed in the cross-sectional TEM measurement, while the BW interface with the quite low $D_{it}$ was abrupt without disorder. The order of $D_{it}$, DHF$\gg$O/E$\gg$BW, predicts the degrees of disorder with DHF$>$O/E$>$BW, which is consistent with the results on the surface and interface observations. Since the densities of interface states obtained from the inset of Fig. 5 are total densities including MIGS, a possible density of MIGS in the metal/6H-SiC(0001) interfaces is extremely lower than the total BW density of $4.63\times 10^{10}$ states$\cdot$cm$^{-2}\cdot$eV$^{-1}$ whose main component is ascribed to that of the disorder induced gap states.

The model for the disorder induced gap states was proposed by Hasegawa and Ohno.[75] Their model assumes the interface disorder is amorphous, thus resulting in the model with a U-shaped energy distribution for $D_{it}$. They called their model DIGS, to which the disorder induced gap state was abbreviated. As discussed already, disorder observed in the metal/6H-SiC(0001) interfaces has the constant energy distributions in $D_{it}$ in the measured energy ranges. Since we measured no $D_{it}$ at the upper and lower edges of the band gap in our experiment due to the limitation of the metal work function range we used, it may have two tails increasing towards the two edges. The constant feature of $D_{it}(E)$ is valid without any assumption in our observed energy ranges. Regardless of inconsistency in the shapes of the energy distributions, the disorder-induced feature by itself is common in both the DIGS model and the experimentally found DIGS. The shapes are subsidiary. Thus, these DIGS can be classified in the same category, which might be called a general DIGS model. For DIGS in our observations, the three interfaces of DHF, O/E, and BW treatments have the same type of disorder in terms of having a unique $\phi_0$.

Further, the relation between the interface structure and the observed DIGS is discussed. In the DHF-treated surface

and interface, a disordered layer was observed in the SiC lattice. In the O/E treatment, however, the disordered layer was etched by the O/E etching process, resulting in the appearance of the periodical $(1\times1)$ surface. Since the thickness of the disordered layer and the oxidized layer after oxidation were 2 nm and 10 nm, respectively, the initial disordered layer was removed completely by the O/E treatment. Even after the removal of the disordered layer, $D_{it}$ was still a value of $2.71\times10^{12}$ states$\cdot$cm$^{-2}\cdot$eV$^{-1}$. Since the SiC layer is an epitaxial crystal, it is reasonable that the residual $D_{it}$ must be attributed to the surface disorder that generates the broad $D_{it}(E)$ distribution and has the observed $\phi_0$. The residual $D_{it}$ was further reduced by BW treatment, implying that surface disorder on the O/E treated surface was removed or passivated. Only from the cross-sectional TEM analysis, no evidence to distinguish removal and passivation was found. In the surface analyses, it is found that an oxygen-related species makes an important role to form a complete reduction of $D_{it}$ in BW treatment. What we observed was the large protrusions along atomic steps. The protrusions can be assigned to the oxygen related species passivating the steps as discussed in Sec. IV. To clarify the behavior of the oxygen-related species, further analyses are needed.

Another important point of view that should be discussed here is homogeneity in electrodes with Schottky barriers. If an electrode in the electrodes has $n=1$, then it has the simplest current transport of thermionic emission over the atop of the barrier height, which is expressed by Eqs. (1) and (2). In a case with a constant $\phi_b$ value with $n=1$ for all the electrodes, they obey the simplest current transport. This is a set of electrodes with complete homogeneous current transport with the simplest mechanism of Eqs. (1) and (2). For electrodes with $n>1$ but with barrier heights concentrating to a value, the current transport for each electrode approximately obeys Eq. $(1')$ with the almost constant values of $n$. We observed this kind of electrodes in the DHF-treated ones as shown in Ni electrodes in Fig. 2 and Mo electrodes in Fig. 3. Also for Ti electrodes in Fig. 4(a), a weak but similar trend is found in the DHF plots. The same phenomenon was observed in Pt electrodes.[49] There are two possibilities to satisfy this condition. One is the set of electrodes with a low density of $D_{it}$ and with a small variation in interfacial electronic and/or atomic structure between the electrodes. In other words, there are some internal variations due to $n>1$ in each electrode. Internal inhomogeneity in one electrode has already been discussed as inhomogeneity in barrier height, which is sometimes called parallel diodes.[33–37]

The other is the set of electrodes with inter-electrodes variation in $n$. The inter-electrodes variation itself can be categorized into two types in terms of the amount of $D_{it}$. The first type is that of electrodes with a large density of $D_{it}$ and with barrier heights that tend to be pinned to a value. Since the DHF interfaces were found to have large densities of $D_{it}$ from Fig. 5, they are in this type. Even though there are any possible causes to induce inter-electrodes variations in $n$ and $\phi_b$, which might be due to various kinds of inhomogeneity in sample preparation, these causes are latent and actually ineffective upon varying $n$ and $\phi_b$ because of the large density of $D_{it}$. Thus, from only the concentrated plots no one can conclude that these DHF electrodes are homogeneous in terms of microscopic interface structures. In the DHF interfaces, the variations of $n$ and $\phi_b$ are condensed but clearly present in narrow ranges shown in the insets of Figs. 2 and 3. The second type of inter-electrodes variation is that with a large variation in $n$ and $\phi_b$ but with a good linearity between $n$ and $\phi_b$. This is seen in unpinned BW interfaces in our experiment. In this kind of unpinned interface, any process-dependent inhomogeneous factor to induce interface states and resultant interface charges is much enhanced due to the low total density of $D_{it}$ and thus the barrier height becomes more sensitive to imperfective homogeneity in the fabrication process to form the interface. If an advanced fabrication process to form a more perfect homogeneous interface with a low density of $D_{it}$ enough to unpin is developed, the distribution of $n-\phi_b$ plots will shift and concentrate toward the ideal value of $\phi_{b0}^{\cdot IV}$.

The linear $\phi_b-n$ relations observed in the DHF, O/E, and BW interfaces and the existence of their unique ideal barrier heights at $n=1$ indicate that the populations of $\phi_b-n$ plots involve a regularity common to each set of electrodes. Since the barrier height is extrapolated into $\phi_{b0}^{\cdot IV}$, it is reasonable that the barrier height in most area of an electrode is $\phi_{b0}^{\cdot IV}$. There might be a possibility that barrier heights at the edges of the electrodes being different from $\phi_{b0}^{\cdot IV}$. To clarify the origin of linear $\phi_b-n$ relations, an advanced study with edge-passivation technique will be needed.

The charge distribution model at the metal/SiC interface is also another significant issue. A simple model on charge distribution proposed by Cowley and Sze[40] has been widely used in calculating $D_{it}$ to know a chemical trend in Schottky barriers.[3,9,34] The advantage of this model is that interface charges are simply categorized into three kinds of charges: the space charge $Q_{sc}$ from ionized impurities in the bulk semiconductor, the charge $Q_{it}$ from the interface states on the semiconductor, and the charge $Q_m$ on the metal. This model is based on the following two assumptions: (1) with intimate contact between the metal and the semiconductor and with an interfacial layer of atomic dimensions, (2) the interface states per unit area per electron volt at the interface are a property of the semiconductor surface and are independent of the metal. Although the model is simple, intimate, and useful for the $D_{it}$ calculation, almost all practical interface systems formed previously satisfied only either of the two assumptions at best. Most abrupt interface systems had quite high dependences of the Schottky barrier heights on preparation conditions of the semiconductor surfaces before metal deposition while there were no interface reaction and diffusion. The barrier heights were unstable and scattered, which results in inadequate qualities to analyze chemical trends at the interfaces. Also in the silicide/Si interface systems that have exceptionally-abrupt interfaces formed by interface reaction of metal/Si interfaces, the densities of interface states strongly depend on interface chemical bonding whose main bonding states are within the band gap,[76] indicating that the interfaces are incompatible with the model.

In the metal/6H-SiC(0001) interface systems formed in our study, the two assumptions are satisfied as described in

the following discussion. As shown in Fig. 16(a), the BW-treated interface is abrupt in atomic scale and the deposited Ti is grown epitaxially on the SiC crystal. As discussed in Sec. V, both of the SiC crystal and the fcc-Ti crystal have perfect crystallinity at the interface and they have a commensurate relation with each other. Thus, the interface spacing between the SiC and Ti crystals should be in the order of the chemical bonding length between interface atoms. Since the topmost atoms of the SiC surface is Si as found in Sec. IV of the surface characterization, Si and Ti atoms should form interface chemical bonds. As discussed in Sec. V, hydrogen atoms that had terminated the terraces of the BW surface desorbed during the Ti deposition. Also, in contrast with a common pinned interface with many dangling bonds and with a resultant $D_{it}$ of $\sim 10^{15}$ states$\cdot$cm$^{-2}\cdot$eV$^{-1}$, the BW interface has a small $D_{it}$ with the order of $10^{10}$ states$\cdot$cm$^{-2}\cdot$eV$^{-1}$. This low $D_{it}$ corresponds to a low density of dangling states, indicating that most bonding states are out of the band gap to form strong chemical bonds. This abrupt and chemically-bonded interface with atomic-scale interface spacing satisfies the assumption (1). As the features of the metal/6H-SiC(0001) interfaces we study, it is stressed that the interface chemical bonding has no influence on $D_{it}(E)$ and $D_{it}(E)$ is determined by the degree of the surface disorder of the SiC crystal.

Next, from Eq. (7) and $S_{\phi}^{\cdot}=\partial\phi_{b0}^{\cdot}/\partial\phi_m$, $D_{it}$ is expressed as the function of $\partial\phi_{b0}^{\cdot}/\partial\phi_m$ as follows:

$$D_{it}=\frac{\varepsilon_i}{q_2\delta}\left(\frac{\partial\phi_m}{\partial\phi_{b0}^{\cdot}}-1\right). \quad (9)$$

Thus, the strong linearity between the metal work function $\phi_m$ and the Schottky barrier height $\phi_{b0}^{\cdot}$ in Fig. 5 directly corresponds to the constancy of $D_{it}$, indicating no influence of the metal on $D_{it}$. In our experiments, changes in $D_{it}$ were observed only when we changed the surface treatments. Also, since the origin of $D_{it}$ is the residual disorder in the SiC crystal, $D_{it}$ is independent of the metal. Therefore, the metal/6H-SiC(0001) interfaces formed by BW, O/E, and DHF treatments satisfies assumption (2). Here, it should be noticed that the linear relation between $\phi_m$ and $\phi_{b0}^{\cdot}$ is a sufficient condition to satisfy assumption (2). The necessary condition for (2) is the absence of dependence of $D_{it}$ on the metal. The significant point of view at the interfaces is that the metals have the role of charge supplier into the interface, not the role of varying $D_{it}$. Thus a system with a predominant MIGS density inherently induced by the metal is incompatible with the model.

Further, as shown in the inset of Fig. 6, we have a strong linear relation without detectable bending between the $1/C^2$ and the applied voltage $V$. This indicates that $Q_{it}$ is constant for varying $V$. In other words, the interface $E_{\mathrm{F}}$ under $V$ applied, which is called the quasi-Fermi level,[1] is fixed. The constant $Q_{it}$ for $V$ supports the applicability of the model for the systems even under a nonequilibrium condition.

From the discussion above, it is found that the metal/6H-SiC(0001) interface system formed by BW, O/E, and DHF treatments is one of the quite simple systems to which the model of Cowley and Sze is applicable. We emphasize that the model is essentially a general model independent of the origin of $D_{it}$. It is also important that the model is inapplicable to an interface system in which the metal and the semiconductor form inherent dangling bonds whose density and energetic distribution depend on the interface structure. Further, in an interface system with many residual interface states that originate from the surface states of the semiconductor, the barrier heights are uncontrollable and lack of reproducibility, thus leading to the inapplicability of the model.

## VII. CONCLUSION

In this work, metal/6H-SiC(0001) interfaces exhibiting the Schottky limit condition were formed and a wide control of the Schottky barrier height were demonstrated. The barrier heights were controlled by changing the deposited metals and by changing surface cleaning procedures. By following a procedure including thermal oxidation followed by HF etching (O/E treatment) and subsequent immersion into boiling pure water before the interface formation took place (BW treatment), the SiC surface was electronically passivated perfectly. For the interfaces formed using this perfectly passivated SiC surface, the density of interface states $D_{it}$ was at the very low value of $4.63\times 10^{10}$ states$\cdot$cm$^{-2}$ eV$^{-1}$. This value is almost three orders lower than that for interfaces prepared by a conventional simple diluted HF-dip (DHF) cleaning treatment. It is concluded that $D_{it}$ and the experimental parameter $S_{\phi}$ from which $D_{it}$ is derived strongly depend on the surface preparation procedure, especially on the perfectivities of the surface atomic arrangement and surface passivation.

The BW-treated SiC surface was hydrogen terminated, with only a small amount of residual oxygen, $<5\%$, which passivated the atomic step edges strongly. For nonboiling water processes of DHF and O/E with the high densities of interface states, a disordered structure was found at the interface. The interface disorder originated from residual disorder of the SiC surface in the nonboiling water processes.

Further, the validity of the $\phi_b-n$ relationship is demonstrated in the metal/6H-SiC interfaces. One can accurately estimate the ideal $\phi_{b0}^{\cdot IV}$ value with an ideal homogeneous thermionic current by means of extrapolating the relationship to $n=1$. This ideal $\phi_{b0}^{\cdot IV}$ coincides with the barrier height measured by the $C-V$ method. $\phi_{b0}^{\cdot IV}$ tells us the real dependence of $\phi_b$ on the metal work function, and thereby an accurate density of interface states is evaluated. From the precise control and estimation of $D_{it}$, a practical charge neutrality level (CNL) of 6H-SiC crystal was found to lie at an energy level of 0.797 V below the conduction band minimum.

## ACKNOWLEDGMENTS

The authors would like to acknowledge Dr. H. Okushi and Dr. K. Kajimura for their financial support and J. Kitamura and Y. Sugawara for their technical support in STM and TEM measurements, respectively. Also, we would like to acknowledge Dr. N. Shibata and Professor Y. Ikuhara for fruitful discussions.

*Present address: Department of Electrical Engineering, Graduate School of Engineering, Osaka University, 2-1 Yamada-oka Suita, Osaka 565-0871, Japan.

†Electronic mail: shiro-hara@aist.go.jp

[1] E. H. Rhoderick and R. H. Williams, *Metal-Semiconductor Contacts*, 2nd ed. (Clarendon, Oxford, 1988).

[2] S. M. Sze, *Physics of Semiconductor Devices*, 2nd ed. (Wiley, New York, 1981).

[3] M. Schlüter, Phys. Rev. B **17**, 5044 (1978). Traditionally, the factor $S_X(\equiv \partial\phi_b/\partial X_m = \partial\phi_b/\partial\phi_m \cdot \partial\phi_m/\partial X_m = AS_\phi)$ was used, where $X_m$ is the electronegativity of a metal. The conversion factor $A(=\partial\phi_m/\partial X_m)$ is 2.27.

[4] S. Kurtin, T. C. McGill, and C. A. Mead, Phys. Rev. Lett. **22**, 1433 (1969).

[5] B. L. Sharma and S. C. Gupta, Solid State Technol. **23**, 97 (1980); and **23**, 900 (1980).

[6] M. S. Tyagi, in *Metal-Semiconductor Schottky Barrier Junctions and Their Applications*, edited by B. L. Sharma (Plenum, New York, 1984), Chap. 1.

[7] V. Heine, Phys. Rev. **138**, A1689 (1965).

[8] J. Tersoff, Phys. Rev. Lett. **52**, 465 (1984).

[9] S. G. Louie, J. R. Chelikowsky, and M. L. Cohen, Phys. Rev. B **15**, 2154 (1977).

[10] To know how to understand MIGS models and experimental works, see a review paper of R. T. Tung, Mater. Sci. Eng. R **35**, 1 (2001).

[11] R. T. Tung, Phys. Rev. Lett. **52**, 461 (1984).

[12] G. Le Lay, V. Yu Aristov, K. Hricovini, A. Taleb-Ibrahimi, P. Dumas, R. Gunther, J. Osvald, and G. Indlekofer, in *Control of Semiconductor Interfaces*, Proceedings of the 1st International Symposium on Control of Semiconductor Interfaces, edited by I. Ohdomari, M. Oshima, and A. Hiraki (Elsevier, Amsterdam, 1994), p. 39.

[13] J. F. Fan, H. Oigawa, and Y. Nannichi, Jpn. J. Appl. Phys. **27**, L2125 (1988).

[14] S. Chang, L. J. Brillson, Y. J. Kime, D. Rioux, P. D. Kirchner, G. D. Pettit, and J. M. Woodall, Phys. Rev. Lett. **64**, 2551 (1990); R. E. Viturro, S. Chang, J. L. Shaw, C. Mailhiot, L. J. Brillson, A. Terrasi, Y. Hwu, G. Margaritondo, P. D. Kirchner, and J. M. Woodall, J. Vac. Sci. Technol. B **7**, 1007 (1989).

[15] K. Shenai, R. S. Scott, and B. J. Baliga, IEEE Trans. Electron Devices **36**, 1811 (1989).

[16] Advances on the SiC studies until the mid-1990's has been published as the issues of review articles as *Special issue on fundamental questions and application of SiC* (Part I), edited by W. J. Choyke, H. Matsunami, and G. Pensl, Phys. Status Solidi B **202**, 1 (1997); *ibid.* (Part II), Phys. Status Solidi A **162**, 1 (1997).

[17] J. R. Waldrop, R. W. Grant, Y. C. Wang, and R. F. Davis, J. Appl. Phys. **72**, 4757 (1992).

[18] J. R. Waldrop and R. W. Grant, Appl. Phys. Lett. **62**, 2685 (1993).

[19] L. M. Porter, R. F. Davis, J. S. Bow, M. J. Kim, and R. W. Carpenter, J. Mater. Res. **10**, 26 (1995).

[20] L. M. Porter, R. F. Davis, J. S. Bow, M. J. Kim, R. W. Carpenter, and R. C. Glass, J. Mater. Res. **10**, 668 (1995).

[21] L. M. Porter, R. F. Davis, J. S. Bow, M. J. Kim, and R. W. Carpenter, J. Mater. Res. **10**, 2336 (1995).

[22] L. M. Porter and R. F. Davis, Mater. Sci. Eng., B **34**, 83 (1995).

[23] W. Kern and D. A. Puotinen, RCA Rev. **31**, 187 (1970).

[24] U. Starke, Ch. Bram, P. -R. Steiner, W. Hartner, L. Hammer, K. Heinz, and K. Müller, Appl. Surf. Sci. **89**, 175 (1995).

[25] S. Watanabe, M. Shigeno, N. Nakayama, and T. Ito, Jpn. J. Appl. Phys. **30**, 3575 (1991).

[26] S. Watanabe and Y. Sugita, Surf. Sci. **327**, 1 (1995).

[27] H. A. Bethe, MIT Radiat. Lab. Rep. 43-12, (1942).

[28] L. Patrick and W. J. Choyke, Phys. Rev. B **2**, 2255 (1970).

[29] T. E. Tiwald, J. A. Woollam, S. Zollner, J. Christiansen, R. B. Gregory, T. Wetteroth, S. R. Wilson, and A. R. Powell, Phys. Rev. B **60**, 11464 (1999).

[30] M. Schadt, G. Pensl, R. P. Devaty, W. J. Choyke, R. Stein, and D. Stephani, Appl. Phys. Lett. **65**, 3120 (1994).

[31] W. Suttrop, G. Pensl, W. J. Choyke, R. Stein, and S. Leibenzeder, J. Appl. Phys. **72**, 3708 (1992).

[32] D. E. Eastman, Phys. Rev. B **2**, 1 (1970); R. M. Eastment and C. H. B. Mee, J. Phys. F: Met. Phys. **3**, 1738 (1973); D. M. Collins, J. B. Lee, and W. E. Spicer, Surf. Sci. **55**, 389 (1976), R. M. Eastment and C. H. B. Mee, J. Phys. F: Met. Phys. **3**, 1738 (1973).

[33] I. Ohdomari, T. S. Kuan, and K. N. Tu, J. Appl. Phys. **50**, 7020 (1979).

[34] R. F. Schmitsdorf, T. U. Kampen, and W. Mönch, Surf. Sci. **324**, 249 (1995); W. Mönch, J. Vac. Sci. Technol. B **17**, 1867 (1999).

[35] D. Defives, O. Noblanc, C. Dua, C. Brylinski, M. Barthula, V. Aubry-Fortuna, and F. Meyer, IEEE Trans. Electron Devices **46**, 449 (1999).

[36] I. Ohdomari and H. Aochi, Phys. Rev. B **35**, 682 (1987).

[37] R. T. Tung, Phys. Rev. B **45**, 13509 (1992).

[38] T. Teraji, S. Hara, H. Okushi, and K. Kajimura, Mater. Res. Soc. Symp. Proc. **423**, 149 (1996).

[39] T. Teraji, S. Hara, H. Okushi, and K. Kajimura, Appl. Phys. Lett. **71**, 689 (1997).

[40] A. M. Cowley and S. M. Sze, J. Appl. Phys. **36**, 3212 (1965).

[41] O. Madelung, *Semiconductors—Basic Data*, 2nd ed. (Springer-Verlag, Berlin, 1996).

[42] S. Yoshida, K. Sasaki, E. Sakuma, S. Misawa, and S. Gonda, Appl. Phys. Lett. **46**, 766 (1985).

[43] S. Hara, T. Teraji, H. Okushi, and K. Kajimura, Appl. Surf. Sci. **117/118**, 394 (1997).

[44] S. Hara, T. Teraji, H. Okushi, and K. Kajimura, Mater. Res. Soc. Symp. Proc. **427**, 159 (1996).

[45] V. V. Afanas'ev, M. Bassler, G. Pensl, M. J. Schulz, and E. Stein von Kamienski, J. Appl. Phys. **79**, 3108 (1996).

[46] R. Williams, Phys. Rev. A **140**, 569 (1965).

[47] J. Pelletier, D. Gervais, and C. Pomot, J. Appl. Phys. **55**, 994 (1984).

[48] W. Mönch, *Semiconductor Surfaces and Interfaces*, 2nd ed. (Springer-Verlag, Berlin, 1995).

[49] S. Hara, Surf. Sci. **494**, L805 (2001).

[50] H. W. Yeom, I. Matsuda, Y. -C. Chao, S. Hara, S. Yoshida, and R. I. G. Uhrberg, Phys. Rev. B **61**, R2417 (2000).

[51] S. W. King, R. J. Nemanich, and R. F. Davis, J. Electrochem. Soc. **146**, 1910 (1999).

[52] L. E. Davis, N. C. MacDonald, P. W. Palmberg, G. E. Riach, and R. E. Weber, *Handbook of Auger Electron Spectroscopy* (Physical Electronics Industries, Eden Prairie, Minnesota, 1976).

[53] V. van Elsbergen, T. U. Kampen, and W. Mönch, Surf. Sci. **365**, 443 (1996).

[54] V. van Elsbergen, O. Janzen, and W. Mönch, Mater. Sci. Eng. B **46**, 366 (1997).

[55] K. Oura and T. Hanawa, Surf. Sci. **82**, 202 (1979).
[56] R. Kaplan, Surf. Sci. **215**, 111 (1989).
[57] V. M. Bermudez, Appl. Surf. Sci. **84**, 45 (1995).
[58] L. I. Johansson, F. Owman, and P. Mårtensson, Surf. Sci. **360**, L478 (1996).
[59] V. Ramachandran and R. M. Feenstra, Phys. Rev. Lett. **82**, 1000 (1999).
[60] J. Furthmüller, F. Bechstedt, H. Hüsken, B. Schröter, and W. Richter, Phys. Rev. B **58**, 13712 (1998).
[61] U. Starke, J. Schardt, J. Bernhardt, M. Franke, K. Reuter, H. Wedler, K. Heinz, J. Furthmüller, P. Käckell, and F. Bechstedt, Phys. Rev. Lett. **80**, 758 (1998).
[62] J. E. Northrup and J. Neugebauer, Phys. Rev. B **52**, R17001 (1995).
[63] S. Hara, Y. Aoyagi, M. Kawai, S. Misawa, E. Sakuma, and S. Yoshida, Surf. Sci. Lett. **278**, L141 (1992).
[64] L. I. Johansson, F. Owman, and P. Mårtensson, Phys. Rev. B **53**, 13793 (1996).
[65] F. Owman and P. Mårtensson, Surf. Sci. **330**, L639 (1995).
[66] S. Tanaka, R. S. Kern, R. F. Davis, J. F. Wendelken, and J. Xu, Surf. Sci. **350**, 247 (1996).
[67] T. Ueda, H. Nishino, and H. Matsunami, J. Cryst. Growth **104**, 695 (1990).
[68] J. Bardeen, Phys. Rev. **71**, 717 (1947).
[69] H. Tsuchida, I. Kamata, and K. Izumi, Appl. Phys. Lett. **70**, 3072 (1997).
[70] H. R. Philipp and E. A. Taft, *Silicon Carbide—A High Temperature Semiconductor*, edited by J. R. O'Connor and J. Smiltens (Pergamon, Oxford, 1960), p. 366.
[71] Y. Sugawara, N. Shibata, S. Hara, and Y. Ikuhara, J. Mater. Res. **15**, 2121 (2000).
[72] A. A. Saleh, V. Shutthanandan, and R. J. Smith, Phys. Rev. B **49**, 4908 (1994).
[73] A. A. Saleh, V. Shutthanandan, N. R. Shivaparan, and R. J. Smith, Phys. Rev. B **56**, 9841 (1997).
[74] The charge neutrality level (CNL), $\phi_0$ is a boundary level between acceptor-like interface states often located in the upper part of the band gap and donor-like interface states often located in the lower part. Consider a condition that the Fermi level at the interface is located just at $\phi_0$. In this condition, the acceptor-like states are empty and the donor-like states are filled. Thus, both the states are uncharged and electrically neutral, which is the reason this level is called CNL. Note that interface charges from the metal side and the bulk ion charges from impurities fixed in the semiconductor due to a band bending as well as the charges from the two type of interface states should be counted when the total charge condition is considered.
[75] H. Hasegawa and H. Ohno, J. Vac. Sci. Technol. B **4**, 1130 (1986).
[76] R. T. Tung, Phys. Rev. Lett. **52**, 461 (1984).